Inclusive quasielastic charged-current neutrino-nucleus reactions

J. Nieves, J. E. Amaro, and M. Valverde
Departamento de Física Moderna, Universidad de Granada, E-18071 Granada, Spain
(Received 1 August 2004; published 30 November 2004)

The quasielastic (QE) contribution of the nuclear inclusive electron scattering model developed by Gil, Nieves, and Oset [Nucl. Phys. **A627**, 543 (1997); **A627**, 599 (1997)] is extended to the study of electroweak charged current (CC) induced nuclear reactions, at intermediate energies of interest for future neutrino oscillation experiments. The model accounts for, among other nuclear effects, long range nuclear [random phase approximation (RPA)] correlations, final state interaction (FSI), and Coulomb corrections. Predictions for the inclusive muon capture in ^{12}C and the reaction $^{12}\mathrm{C}\ (\nu_\mu,\mu^-)X$ near threshold are also given. RPA correlations are shown to play a crucial role and their inclusion leads to one of the best existing simultaneous description of both processes, with accuracies of the order of 10–15 % for the muon capture rate and even better for the Liquid Scintillating Neutrino Detector (LSND) measurement.

DOI: 10.1103/PhysRevC.70.055503 PACS number(s): 25.30.Pt, 13.15.+g, 24.10.Cn, 21.60.Jz

I. INTRODUCTION

The neutrino-induced reactions in nuclei at intermediate energies play an important role in the study of neutrino properties and their interaction with matter [1]. A good example of this is the search for neutrino oscillations, and hence physics beyond the standard model [2]. Several experiments are planned or under construction [1], aimed at determining the neutrino oscillation parameters with high precision. The data analysis will be sensitive to sources of systematic errors, among them nuclear effects at intermediate energies (nuclear excitation energies ranging from about 100 MeV to 500 or 600 MeV), being then of special interest to come up with a unified many-body framework (MBF) in which the electroweak interactions with nuclei could be systematically studied. Such a framework would necessarily include three different contributions: (i) quasielastic (QE) processes, (ii) pion production and two-body processes from the QE region to that beyond the $\Delta(1232)$ resonance peak, and (iii) double pion production and higher nucleon resonance degrees of freedom induced processes. Any model aiming at describing the interaction of neutrinos with nuclei should be first tested against the existing data of interaction of real and virtual photons with nuclei. The literature is rich on this subject, but the only model that has been successfully compared with data at intermediate energies and that systematically includes the first and the second of the contributions, and partially also the third one, mentioned above, is the model developed in Refs. [3] (real photons), and [4] (virtual photons). This model is able to describe inclusive electron-nucleus scattering, total nuclear photoabsorption data, and also measurements of photo- and electronuclear production of pions, nucleons, pairs of nucleons, pion-nucleon pairs, etc. The building blocks of this model are (1) a gauge invariant model for the interaction of real and virtual photons with nucleons, mesons, and nucleon resonances with parameters determined from the vacuum data, and (2) a microscopic treatment of nuclear effects, including long and short range nuclear correlations [5], a final state interaction (FSI), explicit meson and $\Delta(1232)$ degrees of freedom, two and even three nucleon absorption channels, etc. The nuclear effects are computed starting from a local Fermi gas (LFG) picture of the nucleus, and their main features, expansion parameter, and all sorts of constants are completely fixed from previous hadron-nucleus studies (pionic atoms, elastic and inelastic pion-nucleus reactions, Λ hypernuclei, etc.) [6]. The photon coupling constants are determined in the vacuum, and the model has no free parameters. The results presented in Refs. [3,4] are predictions deduced from the framework developed in Refs. [5,6]. One might think that the LFG description of the nucleus is poor, and that a proper finite nuclei treatment is necessary. For inclusive processes and nuclear excitation energies of at least 100 MeV or higher, the findings of Refs. [4,3,6] clearly contradict this conclusion. The reason is that in these circumstances one should sum up over several nuclear configurations, both in the discrete and in the continuum, and this inclusive sum is almost not sensitive to the details of the nuclear wave function, in sharp contrast to what happens in the case of exclusive processes where the final nucleus is left in a determined nuclear level. On the other hand, the LFG description of the nucleus allows for an accurate treatment of the dynamics of the elementary processes (interaction of photons with nucleons, nucleon resonances, and mesons, interaction between nucleons or between mesons and nucleons, etc.), which occur inside the nuclear medium. Within a finite nuclei scenario, such a treatment becomes hard to implement, and often the dynamics is simplified in order to deal with more elaborate nuclear wave functions. This simplification of the dynamics cannot lead to a good description of nuclear inclusive electroweak processes at the intermediate energies of interest for future neutrino oscillation experiments.

Our aim is to extend the nuclear inclusive electron scattering model of Ref. [4], including the axial charged current (CC) degrees of freedom, to describe neutrino- and antineutrino-induced nuclear reactions. This is a long range project; in this work we present our model for the QE region, and hence it constitutes the first step towards this end. We also present results for the inclusive muon capture in ^{12}C and predictions for the Liquid Scintillating Neutrino Detector (LSND) measurement of the reaction $^{12}\mathrm{C}\ (\nu_\mu,\mu^-)X$ near

 ©2004 The American Physical Society

threshold. Both processes are clearly dominated by the QE contribution and are drastically affected by the inclusion of nuclear correlations of the RPA type. We find

$$\Gamma\left[{}^{12}_{\mu^-}\mathrm{C}\right] = 3.2 \times 10^4\ \mathrm{s}^{-1},\quad \overline{\sigma}(\nu_\mu) = 11.9 \times 10^{-40}\ \mathrm{cm}^2, \quad (1)$$

in good agreement with data (discrepancies of the order of 10–15 % for the muon capture rate), despite that those measurements involve extremely low nuclear excitation energies [smaller than 15–20 (25–30) MeV in the first (second) case], where the LFG picture of the nucleus might break down. However, it turns out that the present model provides one of the best existing combined description of these two low-energy measurements, which increases our confidence on the QE predictions of the model at the higher transferred energies of interest for future neutrino experiments. Some preliminary results were presented in Ref. [7].

There is a rich literature both on the inclusive muon capture in nuclei [8–18], and on the CC neutrino-nucleus cross section in the QE region [14–31]. Among all these works, we would like to highlight those included in Refs. [12] (μ capture) and [21] (CC QE scattering) by Oset and collaborators. The framework presented in these works is quite similar to that employed here. Nicely done and in a very simple manner, these works show the most important features of the strong nuclear renormalization effects affecting the nuclear weak responses in the QE region. The main differences with the work presented here concern to the RPA resummation, which, and as consequence of the acquired experience in the inclusive electron scattering studies [4], is here improved, by considering effects not only in the vector-isovector channel of the nucleon-nucleon interaction, but also in the scalar-isovector one. Besides, a more complete tensorial treatment of the RPA response function is also carried out in this work, leading all of these improvements to a better agreement with data. In addition, here we also evaluate the FSI effects for intermediate nuclear excitation energies, not taken into account in the works of Ref. [21], on the neutrino-induced nuclear cross sections.

The paper is organized as follows. After this introduction, we deduce the existing relation among the CC neutrino inclusive nuclear cross sections and the gauge boson W self-energy inside the nuclear medium (Sec. II). In Secs. III and IV we study in detail the QE contribution to the neutrino and antineutrino nuclear cross section, paying special attention to the role played by the strong renormalization of the CC in the medium (Sec. III A) and to the FSI effects (Sec. III C). The inclusive muon capture in nuclei and the relation of this process with inclusive neutrino-induced reactions are examined in Sec. V. The results and main conclusions of this work are compiled in Secs. VI and VII. Finally, in the Appendixes, some detailed formulae are given.

II. CC NEUTRINO INCLUSIVE NUCLEAR REACTIONS

A. General formulae

We will focus on the inclusive nuclear reaction driven by the electroweak CC,

$$\nu_l(k) + A_Z \to l^-(k') + X, \quad (2)$$

though the generalization of the obtained expressions to antineutrino induced reactions, neutral current processes, or inclusive muon capture in nuclei is straightforward. The double differential cross section, with respect to the outgoing lepton kinematical variables, for the process of Eq. (2) is given in the laboratory frame by

$$\frac{d^2\sigma_{\nu l}}{d\Omega(\hat{k}')dE_l'} = \frac{|\vec{k}'|}{|\vec{k}|}\frac{G^2}{4\pi^2}L_{\mu\sigma}W^{\mu\sigma} \quad (3)$$

with $\vec{k}$ and $\vec{k}'$ the laboratory lepton momenta, $E_l' = (\vec{k}'^2 + m_l^2)^{1/2}$ and m_l the energy and the mass of the outgoing lepton ($m_\mu = 105.65$ MeV, $m_e = 0.511$ MeV), respectively, $G = 1.1664 \times 10^{-11}$ MeV^{-2}, the Fermi constant, and L and W the leptonic and hadronic tensors, respectively. The leptonic tensor is given by [in our convention, we take $\epsilon_{0123} = +1$ and the metric $g^{\mu\nu} = (+,-,-,-)$]:

$$L_{\mu\sigma} = L^s_{\mu\sigma} + iL^a_{\mu\sigma} = k'_\mu k_\sigma + k'_\sigma k_\mu - g_{\mu\sigma}k\cdot k' + i\epsilon_{\mu\sigma\alpha\beta}k'^\alpha k^\beta. \quad (4)$$

The hadronic tensor includes all sort of nonleptonic vertices and corresponds to the charged electroweak transitions of the target nucleus, i, to all possible final states. It is thus given by[1]

$$W^{\mu\sigma} = \frac{1}{2M_i}\overline{\sum_f}(2\pi)^3\delta^4(P'_f - P - q)\langle f|j^\mu_{\mathrm{cc}}(0)|i\rangle\langle f|j^\sigma_{\mathrm{cc}}(0)|i\rangle^* \quad (5)$$

with P^μ the four-momentum of the initial nucleus, $M_i = P^2$ the target nucleus mass, P'_f the total four-momentum of the hadronic state f, and $q = k - k'$ the four-momentum transferred to the nucleus. The bar over the sum denotes the average over initial spins, and finally for the CC we take

$$j^\mu_{\mathrm{cc}} = \overline{\Psi}_u\gamma^\mu(1-\gamma_5)(\cos\theta_C\Psi_d + \sin\theta_C\Psi_s) \quad (6)$$

with Ψ_u, Ψ_d, and Ψ_s quark fields, and θ_C the Cabibbo angle ($\cos\theta_C = 0.974$). By construction, the hadronic tensor accomplishes

$$W^{\mu\sigma} = W^{\mu\sigma}_s + iW^{\mu\sigma}_a \quad (7)$$

with $W^{\mu\sigma}_s$ ($W^{\mu\sigma}_a$) real symmetric (antisymmetric) tensors. To obtain Eq. (3) we have neglected the four-momentum carried out by the intermediate W boson with respect to its mass, and have used the existing relation between the gauge weak coupling constant, $g = e/\sin\theta_W$, and the Fermi constant $G/\sqrt{2} = g^2/8M_W^2$, with e the electron charge, θ_W the Weinberg angle, and M_W the W-boson mass.

The hadronic tensor is completely determined by six independent, Lorentz scalar and real, structure functions $W_i(q^2)$,

[1]Note that (i) Eq. (5) holds with states normalized so that $\langle\vec{p}|\vec{p}'\rangle = (2\pi)^3 2p_0\delta^3(\vec{p}-\vec{p}')$, (ii) the sum over final states f includes an integration $\int d^3p_j/((2\pi)^3 2E_j)$, for each particle j making up the system f, as well as a sum over all spins involved.

$$\frac{W^{\mu\nu}}{2M_i} = -g^{\mu\nu}W_1 + \frac{P^\mu P^\nu}{M_i^2}W_2 + i\frac{\epsilon^{\mu\nu\gamma\delta}P_\gamma q_\delta}{2M_i^2}W_3 + \frac{q^\mu q^\nu}{M_i^2}W_4 + \frac{P^\mu q^\nu + P^\nu q^\mu}{2M_i^2}W_5 + i\frac{P^\mu q^\nu - P^\nu q^\mu}{2M_i^2}W_6. \quad (8)$$

Taking $\vec{q}$ in the z direction, i.e., $\vec{q}=|q|\vec{u}_z$, and $P^\mu=(M_i,\vec{0})$, it is straightforward to find the six structure functions in terms of the W^{00}, $W^{xx}=W^{yy}$, W^{zz}, W^{xy}, and W^{0z} components of the hadronic tensor.[2] After contracting with the leptonic tensor we obtain

$$\frac{d^2\sigma_{\nu l}}{d\Omega(\hat{k}')dE_l'} = \frac{|\vec{k}'|E_l'M_iG^2}{\pi^2}\Bigg\{2W_1\sin^2\frac{\theta'}{2} + W_2\cos^2\frac{\theta'}{2} - W_3\frac{E_\nu+E_l'}{M_i}\sin^2\frac{\theta'}{2} + \frac{m_l^2}{E_l'(E_l'+|\vec{k}'|)}\Bigg[W_1\cos\theta' - \frac{W_2}{2}\cos\theta' + \frac{W_3}{2}\left(\frac{E_l'+|\vec{k}'|}{M_i} - \frac{E_\nu+E_l'}{M_i}\cos\theta'\right) + \frac{W_4}{2}\left(\frac{m_l^2}{M_i^2}\cos\theta' + \frac{2E_l'(E_l'+|\vec{k}'|)}{M_i^2}\sin^2\theta'\right) - W_5\frac{E_l'+|\vec{k}'|}{2M_i}\Bigg]\Bigg\} \quad (10)$$

with E_ν the incoming neutrino energy and θ' the outgoing lepton scattering angle. The cross section does not depend on M_i, as can be seen from the relations of Eq. (9), and also note that the structure function W_6 does not contribute.

B. Hadronic tensor and the gauge boson self-energy in the nuclear medium

In our MBF, the hadronic tensor is determined by the W^+-boson self-energy, $\Pi_W^{\mu\rho}(q)$, in the nuclear medium. We follow here the formalism of Ref. [4], and we evaluate the self-energy, $\Sigma_\nu^r(k;\rho)$, of a neutrino, with four-momentum k and helicity r, moving in infinite nuclear matter of density ρ. Diagrammatically this is depicted in Fig. 1, and we get

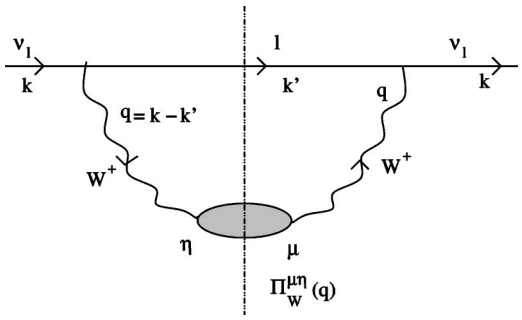

FIG. 1. Diagrammatic representation of the neutrino self-energy in nuclear matter.

$$-i\Sigma_\nu^r(k;\rho) = \int\frac{d^4q}{(2\pi)^4}\overline{u_r}(k)\Bigg\{-i\frac{g}{2\sqrt{2}}\gamma_L^\mu iD_{\mu\alpha}(q)\times[-i\Pi_W^{\alpha\beta}(q;\rho)]iD_{\beta\sigma}(q)i\frac{\not{k}'+m_l}{k'^2-m_l^2+i\epsilon}\times\left(-i\frac{g}{2\sqrt{2}}\right)\gamma_L^\sigma\Bigg\}u_r(k) \quad (11)$$

with $D_{\mu\alpha}(q)=(-g_{\mu\alpha}+q_\mu q_\alpha/M_W^2)/(q^2-M_W^2+i\epsilon)$, $\Pi_W^{\mu\eta}(q;\rho)$ is the virtual W^+ self-energy in the medium, $\gamma_L^\mu=\gamma^\mu(1-\gamma_5)$, and the spinor normalization is given by $\overline{uu}=2m$. Since right-handed neutrinos are sterile, only the left-handed neutrino self-energy, $\Sigma_\nu(k;\rho)$, is not zero and obviously $\Sigma_\nu(k;\rho)=\Sigma_r\Sigma_\nu^r(k;\rho)$. The sum over helicities leads to traces in Dirac's space and thus we get

$$\Sigma_\nu(k;\rho) = \frac{8iG}{\sqrt{2}M_W^2}\int\frac{d^4q}{(2\pi)^4}\frac{L_{\eta\mu}\Pi_W^{\mu\eta}(q;\rho)}{k'^2-m_l^2+i\epsilon}. \quad (12)$$

The neutrino disappears from the elastic flux, by inducing one-particle-one-hole (1p1h), 2p2h,… excitations, $\Delta(1232)$-hole (Δh) excitations, or creating pions, etc., at a rate given by

$$\Gamma(k;\rho) = -\frac{1}{k^0}\,\mathrm{Im}\,\Sigma_\nu(k;\rho). \quad (13)$$

We get the imaginary part of Σ_ν by using Cutkosky's rules. In this case we cut with a straight vertical line (see Fig. 1) the intermediate lepton state and those implied by the W-boson polarization (shaded region). Those states are then placed on the shell by taking the imaginary part of the propagator, self-energy, etc. Thus, we obtain for $k^0>0$

$$\mathrm{Im}\,\Sigma_\nu(k) = \frac{8G}{\sqrt{2}M_W^2}\int\frac{d^3k'}{(2\pi)^3}\frac{\Theta(q^0)}{2E_l'}\,\mathrm{Im}\{\Pi_W^{\mu\eta}(q;\rho)L_{\eta\mu}\} \quad (14)$$

[2]These relations read

$$W_1=\frac{W^{xx}}{2M_i},\ W_2=\frac{1}{2M_i}\left(W^{00}+W^{xx}+\frac{(q^0)^2}{|\vec{q}|^2}(W^{zz}-W^{xx})-2\frac{q^0}{|\vec{q}|}\mathrm{Re}\,W^{0z}\right),$$

$$W_3=-i\frac{W^{xy}}{|\vec{q}|},$$

$$W_4=\frac{M_i}{2|\vec{q}|^2}(W^{zz}-W^{xx}),\ W_5=\frac{1}{|\vec{q}|}\left(\mathrm{Re}\,W^{0z}-\frac{q^0}{|\vec{q}|}(W^{zz}-W^{xx})\right), \quad (9)$$

$$W_6=\frac{\mathrm{Im}\,W^{0z}}{|\vec{q}|}.$$

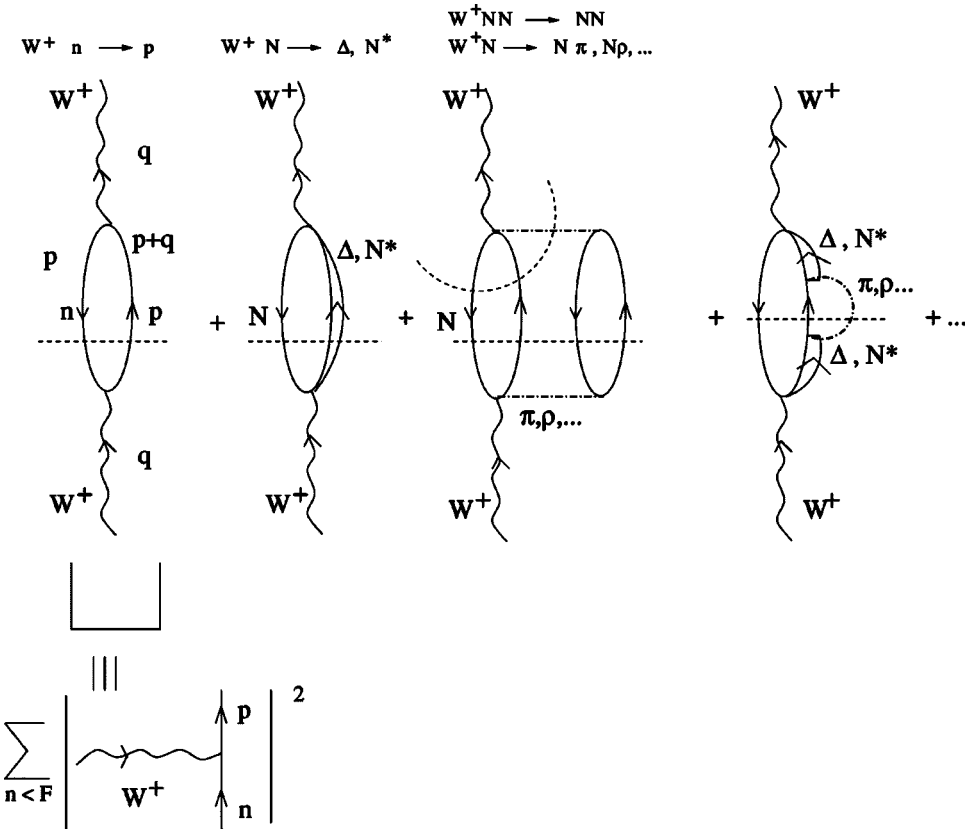

FIG. 2. Diagrammatic representation of some diagrams contributing to the W^+ self-energy.

with $\Theta(\cdots)$ the Heaviside function. Since $\Gamma dtdS$ provides a probability times a differential of area, which is a contribution to the (ν_l, l) cross section, we have

$$d\sigma = \Gamma(k;\rho)dtdS = -\frac{1}{k^0}\,\mathrm{Im}\,\Sigma_\nu(k;\rho)dtdS$$

$$= -\frac{1}{|\vec{k}|}\,\mathrm{Im}\,\Sigma_\nu(k;\rho)d^3r \tag{15}$$

and hence the nuclear cross section is given by

$$\sigma = -\frac{1}{|\vec{k}|}\int \mathrm{Im}\,\Sigma_\nu(k;\rho(r))d^3r, \tag{16}$$

where we have substituted Σ_ν as a function of the nuclear density at each point of the nucleus and integrate over the whole nuclear volume. Hence, we assume the local density approximation, (LDA), which, as shown in Ref. [3], is an excellent approximation for volume processes like the one studied here. Coming back to Eq. (14) we find

$$\frac{d^2\sigma_{\nu l}}{d\Omega(\hat{k}')dk'^0} = -\frac{|\vec{k}'|}{|\vec{k}|}\frac{G^2}{4\pi^2}\left(\frac{2\sqrt{2}}{g}\right)^2\int\frac{d^3r}{2\pi}\{L^s_{\mu\eta}\,\mathrm{Im}(\Pi^{\mu\eta}_W + \Pi^{\eta\mu}_W)$$

$$- L^a_{\mu\eta}\,\mathrm{Re}(\Pi^{\mu\eta}_W - \Pi^{\eta\mu}_W)\}\Theta(q^0) \tag{17}$$

and then by comparing to Eq. (3), the hadronic tensor reads

$$W^{\mu\sigma}_s = -\Theta(q^0)\left(\frac{2\sqrt{2}}{g}\right)^2\int\frac{d^3r}{2\pi}\,\mathrm{Im}[\Pi^{\mu\sigma}_W + \Pi^{\sigma\mu}_W](q;\rho), \tag{18}$$

$$W^{\mu\sigma}_a = -\Theta(q^0)\left(\frac{2\sqrt{2}}{g}\right)^2\int\frac{d^3r}{2\pi}\,\mathrm{Re}[\Pi^{\mu\sigma}_W - \Pi^{\sigma\mu}_W](q;\rho). \tag{19}$$

As we see, the basic object is the self-energy of the gauge boson $(W^\pm)$ inside of the nuclear medium. Following the lines of Ref. [4], we should perform a many-body expansion, where the relevant gauge boson absorption modes would be systematically incorporated: absorption by one nucleon, or a pair of nucleons or even three nucleon mechanisms, real and virtual meson $(\pi, \rho, \ldots)$ production, excitation of Δ of higher resonance degrees of freedom, etc. In addition, nuclear effects such as RPA or short range correlations[3] (SRC) should also be taken into account. Some of the W absorption modes are depicted in Fig. 2.

Up to this point the formalism is rather general and its applicability has not been restricted to the QE region. In this work we will focus on the QE contribution to the total cross section, and it will be analyzed in detail in the next section.

III. QE CONTRIBUTION TO $\Pi^{\mu\nu}_W(q;\rho)$

The virtual W^+ can be absorbed by one nucleon leading to the QE contribution of the nuclear response function. Such a contribution corresponds to a 1p1h nuclear excitation (first of the diagrams depicted in Fig. 2). To evaluate this self-energy, the free nucleon propagator in the medium is required:

[3]For that purpose we use an effective interaction of the Landau-Migdal type.

$$S(p;\rho) = (\not{p} + M)G(p;\rho),$$

$$G(p;\rho) = \left(\frac{1}{p^2 - M^2 + i\epsilon} + \frac{2\pi i}{2E(\vec{p})}\delta(p^0 - E(\vec{p}))\Theta(k_F - |\vec{p}|)\right) \tag{20}$$

with the local Fermi momentum $k_F(r) = [3\pi^2\rho(r)/2]^{1/3}$, $M = 940$ MeV the nucleon mass, and $E(\vec{p}) = \sqrt{M^2 + \vec{p}^2}$. We will work on a nonsymmetric nuclear matter with different Fermi sea levels for protons, k_F^p, than for neutrons, k_F^n (equation above, but replacing $\rho/2$ by ρ_p or ρ_n, with $\rho = \rho_p + \rho_n$). On the other hand, for the W^+pn vertex we take

$$\langle p;\vec{p}\,' = \vec{p} + \vec{q}|j_{cc}^{\alpha}(0)|n;\vec{p}\rangle = \overline{u}(\vec{p}\,')(V^{\alpha} - A^{\alpha})u(p) \tag{21}$$

with vector and axial nucleon currents given by

$$V^{\alpha} = 2(\cos\,\theta_C)\left(F_1^V(q^2)\gamma^{\alpha} + i\mu_V\frac{F_2^V(q^2)}{2M}\sigma^{\alpha\nu}q_{\nu}\right),$$

$$A^{\alpha} = \cos\,\theta_C G_A(q^2)\left(\gamma^{\alpha}\gamma_5 + \frac{2M}{m_{\pi}^2 - q^2}q^{\alpha}\gamma_5\right) \tag{22}$$

with $m_{\pi} = 139.57$ MeV. Partially conserved axial current and invariance under G parity have been assumed to relate the pseudoscalar form factor to the axial one and to discard a term of the form $(p^{\mu} + p'^{\mu})\gamma_5$ in the axial sector, respectively. Invariance under time reversal guarantees that all form factors are real. Besides, due to isospin symmetry, the vector form factors are related to the electromagnetic ones:[4]

$$F_1^V(q^2) = \frac{1}{2}[F_1^p(q^2) - F_1^n(q^2)],$$

$$\mu_V F_2^V(q^2) = \frac{1}{2}[\mu_p F_2^p(q^2) - \mu_n F_2^n(q^2)] \tag{24}$$

and for the axial form factor we use

$$G_A(q^2) = \frac{g_A}{(1 - q^2/M_A^2)^2},\ g_A = 1.257,\ M_A = 1.049\ \text{GeV}. \tag{25}$$

With all of these ingredients it is straightforward to evaluate the contribution to the W^+ self-energy of the first diagram of Fig. 2,

$$-i\Pi_W^{\mu\nu}(q^0,\vec{q}) = -\cos^2\,\theta_C\left(\frac{g}{2\sqrt{2}}\right)^2\int\frac{d^4p}{(2\pi)^4}A^{\mu\nu}(p,q) \times G(p;\rho_n)G(p+q;\rho_p) \tag{26}$$

with the CC nucleon tensor given by

$$A^{\mu\nu}(p,q) = \mathrm{Tr}\left\{\left[2F_1^V\gamma^{\mu} - 2i\mu_V\frac{F_2^V}{2M}\sigma^{\mu\alpha}q_{\alpha} - G_A \times\left(\gamma^{\mu}\gamma_5 - \frac{2M}{m_{\pi}^2 - q^2}q^{\mu}\gamma_5\right)\right](\not{p} + \not{q} + M) \times\left[2F_1^V\gamma^{\nu} + 2i\mu_V\frac{F_2^V}{2M}\sigma^{\nu\beta}q_{\beta} - G_A \times\left(\gamma^{\nu}\gamma_5 + \frac{2M}{m_{\pi}^2 - q^2}q^{\nu}\gamma_5\right)\right](\not{p} + M)\right\}. \tag{27}$$

The Dirac space traces above can be easily done and the nucleon tensor can be found in Appendix A. Subtracting the divergent vacuum contribution in Eq. (26), we finally get from Eqs. (18) and (19)

$$W^{\mu\nu}(q^0,\vec{q}) = -\frac{\cos^2\,\theta_C}{2M^2}\int_0^{\infty}dr r^2 \times\left\{2\Theta(q^0)\int\frac{d^3p}{(2\pi)^3}\frac{M}{E(\vec{p})}\frac{M}{E(\vec{p}+\vec{q})}\Theta(k_F^n(r) - |\vec{p}|)\Theta(|\vec{p}+\vec{q}| - k_F^p(r))(-\pi) \times\delta(q^0 + E(\vec{p}) - E(\vec{p}+\vec{q}))\,A^{\nu\mu}(p,q)|_{p^0 = E(\vec{p})}\right\}. \tag{28}$$

The d^3p integrations above can be analytically done and all of them are determined by the imaginary part of the relativistic isospin asymmetric Lindhard function, $\overline{U_R}(q,k_F^n,k_F^p)$. Explicit expressions can be found in Appendix B.

Up to this point the treatment is fully relativistic and the four-momentum transferred to the nucleus can be comparable or higher than the nucleon mass.[5] At low and intermediate energies, RPA effects become extremely large, as shown, for instance, in Ref. [12]. To account for RPA effects, we will use a nucleon-nucleon effective force [33] determined from calculations of nuclear electric and magnetic moments, transition probabilities, and giant electric and magnetic multipole resonances using a nonrelativistic nuclear dynamics scheme. This force, supplemented by nucleon-$\Delta(1232)$ and $\Delta(1232)$-$\Delta(1232)$ interactions [5,6], was successfully used in the work of Ref. [4] on inclusive nuclear electron scattering. In this latter reference a nonrelativistic LFG is also employed. Thus, it is of interest to discuss also the hadronic tensor of Eq. (28) in the context of a nonrela-

[4]We use the parameterization of Galster and collaborators [32],

$$F_1^N = \frac{G_E^N + \tau G_M^N}{1+\tau},$$

$$\mu_N F_2^N = \frac{G_M^N - G_E^N}{1+\tau}, \tag{23}$$

$$G_E^p = \frac{G_M^p}{\mu_p} = \frac{G_M^n}{\mu_n} = -(1 + \lambda_n\tau)\frac{G_E^n}{\mu_n\tau} = \left(\frac{1}{1 - q^2/M_D^2}\right)^2$$

with $\tau = -q^2/4M^2$, $M_D = 0.843$ GeV, $\mu_p = 2.792\,847$, $\mu_n = -1.913\,043$, and $\lambda_n = 5.6$.

[5]The only limitation on its size is given by possible quark effects, not included in the nucleon form factors of Eqs. (23)–(25).

tivistic Fermi gas. This is easily done by replacing the factors $M/E(\vec{p})$ and $M/E(\vec{p}+\vec{q})$ in Eq. (28) by one. Explicit expressions can be now found in Appendix C.

Pauli blocking, through the imaginary part of the Lindhard function, is the main nuclear effect included in the hadronic tensor of Eq. (28). In the next sections, we will study different nuclear corrections to $W^{\mu\nu}$.

To finish this section, we devote a few words to the low density theorem (LDT). At low nuclear densities the imaginary part of the relativistic isospin asymmetric Lindhard function can be approximated by

$$\mathrm{Im}\,\overline{U_R}(q,k_F^n,k_F^p) \approx -\pi\rho_n \frac{M}{E(\vec{q})}\delta(q^0+M-E(\vec{q})) \quad (29)$$

and thus one readily finds[6]

$$\sigma_{\nu_l+A_Z\to l^-+X} \approx N\sigma_{\nu_l+n\to l^-+p},\ N=A-Z, \quad (31)$$

which is accomplished with the LDT. For future purposes we give in Appendix D the $\nu_l+n\to l^-+p$ differential cross section.

A. RPA nuclear correlations

When the electroweak interactions take place in nuclei, the strengths of electroweak couplings may change from their free nucleon values due to the presence of strongly interacting nucleons [12]. Indeed, since the nuclear experiments on β decay in the early 1970s [34], the quenching of axial current is a well-established phenomenon. We follow here the MBF of Ref. [4], and take into account the medium polarization effects in the 1p1h contribution to the W self-energy by substituting it by an RPA response as shown diagrammatically in Fig. 3. For that purpose we use an effective ph-ph interaction of the Landau-Migdal type,

$$V=c_0\{f_0(\rho)+f_0'(\rho)\vec{\tau}_1\vec{\tau}_2+g_0(\rho)\vec{\sigma}_1\vec{\sigma}_2+g_0'(\rho)\vec{\sigma}_1\vec{\sigma}_2\vec{\tau}_1\vec{\tau}_2\}, \quad (32)$$

where $\vec{\sigma}$ and $\vec{\tau}$ are Pauli matrices acting on the nucleon spin and isospin spaces, respectively. Note that the above interaction is of contact type, and therefore in coordinate space one has $V(\vec{r}_1,\vec{r}_2)\propto\delta(\vec{r}_1-\vec{r}_2)$. As mentioned before, the coefficients were determined in Ref. [33] from calculations of nuclear electric and magnetic moments, transition probabilities, and giant electric and magnetic multipole resonances. They are parametrized as

$$f_i(\rho(r)) = \frac{\rho(r)}{\rho(0)}f_i^{(in)} + \left[1-\frac{\rho(r)}{\rho(0)}\right]f_i^{(ex)}, \quad (33)$$

where

[6]The energy of the outgoing lepton is completely fixed once the Fermi distribution of the nucleons is neglected. Thus all structure functions W_i get the energy conservation Dirac δ into their definition. Indeed, we have

$$W^{\mu\nu}=\frac{N\cos^2\theta_C}{8ME(\vec{q})}\delta(q^0+M-E(\vec{q}))A^{\nu\mu}|_{p=(M,\vec{0})}. \quad (30)$$

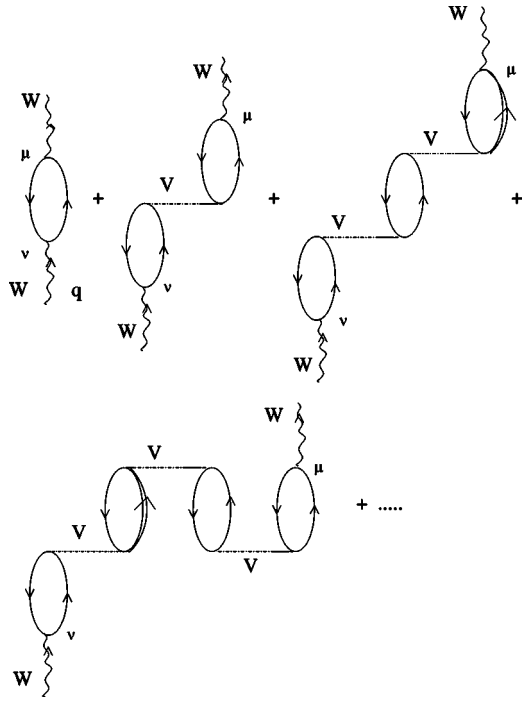

FIG. 3. Set of irreducible diagrams responsible for the polarization (RPA) effects in the 1p1h contribution to the W self-energy.

$$f_0^{(in)}=0.07,\ f_0'^{(ex)}=0.45,$$

$$f_0^{(ex)}=-2.15,\ f_0'^{(in)}=0.33, \quad (34)$$

$$g_0^{(in)}=g_0^{(ex)}=g_0=0.575,\ g_0'^{(in)}=g_0'^{(ex)}=g_0'=0.725,$$

and $c_0=380$ MeV fm^3. In the $S=1=T$ channel ($\vec{\sigma}\vec{\sigma}\vec{\tau}\vec{\tau}$ operator) we use an interaction with explicit π (longitudinal) and ρ (transverse) exchanges, which has been used for the renormalization of the pionic and pion related channels in different nuclear reactions at intermediate energies [3–6]. Thus we replace

$$c_0g_0'(\rho)\vec{\sigma}_1\vec{\sigma}_2\vec{\tau}_1\vec{\tau}_2 \to \vec{\tau}_1\vec{\tau}_2\sum_{i,j=1}^{3}\sigma_1^i\sigma_2^jV_{ij}^{\sigma\tau},$$

$$V_{ij}^{\sigma\tau}=(\hat{q}_i\hat{q}_jV_l(q)+(\delta_{ij}-\hat{q}_i\hat{q}_j)V_t(q)) \quad (35)$$

with $\hat{q}=\vec{q}/|\vec{q}|$, and the strengths of the ph-ph interaction in the longitudinal and transverse channel are given by

$$V_l(q^0,\vec{q})=\frac{f^2}{m_\pi^2}\left\{\left(\frac{\Lambda_\pi^2-m_\pi^2}{\Lambda_\pi^2-q^2}\right)^2\frac{\vec{q}^2}{q^2-m_\pi^2}+g_l'(q)\right\},$$

$$\frac{f^2}{4\pi}=0.08,\ \Lambda_\pi=1200\ \mathrm{MeV},$$

$$V_t(q^0,\vec{q})=\frac{f^2}{m_\pi^2}\left\{C_\rho\left(\frac{\Lambda_\rho^2-m_\rho^2}{\Lambda_\rho^2-q^2}\right)^2\frac{\vec{q}^2}{q^2-m_\rho^2}+g_t'(q)\right\}, \quad (36)$$

$$C_\rho=2,\ \Lambda_\rho=2500\ \mathrm{MeV},\ m_\rho=770\ \mathrm{MeV}.$$

The SRC functions g_l' and g_t' have a smooth q dependence [5,35], which we will not consider here,[7] and thus we will take $g_l'(q)=g_t'(q)=g'=0.63$ as was done in the study of inclusive nuclear electron scattering carried out in Ref. [4], and also in some of the works of Ref. [6]. Note that $c_0 g_0'$ and $g' f^2/m_\pi^2$ differ from each other in less than 10%.

We also include $\Delta(1232)$ degrees of freedom in the nuclear medium, which, given the spin-isospin quantum numbers of the Δ resonance, only modify the vector-isovector ($S=1=T$) channel of the RPA response function. The ph-Δh and Δh-Δh effective interactions are obtained from Eqs. (35) and (36) by replacing $\vec{\sigma}\to\vec{S}$, $\vec{\tau}\to\vec{T}$, where $\vec{S},\vec{T}$ are the spin, isospin $N\Delta$ transition operators [5] and $f\to f^*=2.13f$, for any Δ that replaces a nucleon.

Thus, the V lines in Fig. 3 stand for the effective ph(Δh)-ph(Δh) interaction described so far. Given the isospin structure of the $W^\pm NN$ coupling, the isoscalar terms (f_0 and g_0) of the effective interaction cannot contribute to the RPA response function. We should stress that this effective interaction is nonrelativistic, and then for consistency we will neglect terms of order $O(p^2/M^2)$ when summing up the RPA series.

To start with, let us examine how the axial vector term ($G_A\gamma^\mu\gamma_5\tau_+/2$, where $\tau_\pm=\tau_x\pm i\tau_y$ are the ladder isospin operators responsible for the n to p and p to n transitions, $\tau^+|n\rangle=2|p\rangle$) of the CC axial current is renormalized. As mentioned above, we will only compute the higher density corrections, implicit in the RPA series, to the leading and next-to-leading orders in the p/M expansion. The nonrelativistic reduction of the axial vector term in the nucleon current reads

$$G_A\overline{u}_{r'}(\vec{p}\,')\frac{\tau_+}{2}\gamma^\mu\gamma_5 u_r(p)=2MG_A\chi^\dagger_{r'}\left(-g^{\mu i}\sigma^i+g^{\mu 0}\frac{\vec{\sigma}\cdot(\vec{p}+\vec{p}\,')}{2M}+\cdots\right)\frac{\tau_+}{2}\chi_r,\ i=1,2,3 \tag{37}$$

with $\vec{p}\,'=\vec{p}+\vec{q}$, and χ_r a nonrelativistic nucleon spin-isospin wave function. In Eq. (37) there is a sum on the repeated index i and the dots stand for corrections[8] of order $O(\vec{p}^2/M^2,\vec{p}\,'^2/M^2,q^0/M)$. In the impulse approximation, this current leads to a CC nucleon tensor,[9]

$$A^{\mu\nu}(p,q)|^{NR}_{\text{axial vector}}=8M^2(\mathcal{A}_1^{\mu\nu}+\mathcal{A}_2^{\mu\nu}),$$

$$\mathcal{A}_1^{\mu\nu}=G_A^2 g^{\mu i}g^{\nu j}\delta^{ij}, \tag{38}$$

$$\mathcal{A}_2^{\mu\nu}=-G_A^2(g^{\mu i}g^{\nu 0}+g^{\mu 0}g^{\nu i})\frac{(2\vec{p}+\vec{q})^i}{2M}$$

with $i,j=1,2,3$ and there is again a sum for repeated indices. The tensor $A^{\mu\nu}(p,q)|^{NR}_{\text{axial vector}}$ can be also obtained from the nonrelativistic reduction of $A^{\mu\nu}(p,q)$ in Eq. (A1). The $\mathcal{A}_1$ contribution comes from the leading operator $-g^{\mu i}\sigma^i\tau_+/2$, and involves the trace of $G_A^2\sigma^i\sigma^j$ (1p1h excitation depicted in the first diagram of Fig. 3). Let us consider first this simple operator and only forward propagating (direct term of the Lindhard function) ph excitations. Taking into account the spin structure of this operator the scalar term f_0' of the effective interaction does not contribute either, and thus we are left with the spin-isospin channel of the effective interaction, $\Sigma_{ij}V_{ij}^{\sigma\tau}\sigma_1^i\sigma_2^j\vec{\tau}_1\vec{\tau}_2$. Let us now look at the irreducible diagrams consisting of the excitation of one and two ph states (first and second diagrams of Fig. 3). The contribution of those diagrams to the W self-energy is

$$\begin{aligned}\Pi_W^{ij}&\propto\langle p|\frac{\tau_+}{2}|n\rangle\langle n|\frac{\tau_-}{2}|p\rangle\frac{\overline{U}}{2}\mathrm{Tr}(\sigma^i\sigma^j)+\langle p|\frac{\tau_+}{2}|n\rangle\langle n|\vec{\tau}|p\rangle\langle p|\vec{\tau}|n\rangle\\&\times\langle n|\frac{\tau_-}{2}|p\rangle\left(\frac{\overline{U}}{2}\right)^2\sum_{k,l=1}^{3}\mathrm{Tr}(\sigma^i\sigma^l)\mathrm{Tr}(\sigma^k\sigma^j)V_{lk}^{\sigma\tau}\\&=\overline{U}(q,k_F^n,k_F^p)[\delta^{ij}+2\overline{U}(q,k_F^n,k_F^p)V_{\sigma\tau}^{ij}].\end{aligned} \tag{39}$$

The excitation of three ph states gives a contribution of $\overline{U}(2\overline{U})^2\Sigma_k V_{\sigma\tau}^{ik}V_{\sigma\tau}^{kj}=\overline{U}(2\overline{U})^2[\hat{q}_i\hat{q}_jV_l^2+(\delta_{ij}-\hat{q}_i\hat{q}_j)V_t^2]$ to Π_W^{ij}. Thus, the full sum of multiple ph excitation states, implicit in Fig. 3, leads to two independent geometric series, in the longitudinal and transverse channels, which are taken into account by the following substitution in the hadronic tensor ($W^{\mu\nu}$),

$$\begin{aligned}&\delta^{ij}8M^2G_A^2\ \mathrm{Im}\,\overline{U}(q,k_F^n,k_F^p)\\&\quad\to 8M^2G_A^2\,\mathrm{Im}\left\{\overline{U}(q,k_F^n,k_F^p)\left(\frac{\hat{q}^i\hat{q}^j}{1-2\overline{U}(q,k_F^n,k_F^p)V_l(q)}+\frac{\delta^{ij}-\hat{q}^i\hat{q}^j}{1-2\overline{U}(q,k_F^n,k_F^p)V_t(q)}\right)\right\}\\&\quad=8M^2G_A^2\,\mathrm{Im}\,\overline{U}(q,k_F^n,k_F^p)\left(\frac{\hat{q}^i\hat{q}^j}{|1-2\overline{U}(q,k_F^n,k_F^p)V_l(q)|^2}+\frac{\delta^{ij}-\hat{q}^i\hat{q}^j}{|1-2\overline{U}(q,k_F^n,k_F^p)V_t(q)|^2}\right).\end{aligned} \tag{40}$$

The factor 2 in the denominator above and that in Eq. (39) comes from the isospin dependence, $\vec{\tau}_1\cdot\vec{\tau}_2$, of the effective ph-ph interaction. Taking account of Δh and backward (crossed term of the Lindhard function) propagating ph excitations (see Fig. 3), not accounted for by $\overline{U}$, is readily done by substituting $2\overline{U}$ in the denominator by $U(q,k_F)=U_N+U_\Delta$, the Lindhard function of Ref. [35], which for simplicity we evaluate[10] in an isospin symmetric nuclear medium of density ρ. The different couplings for N and Δ are incorpo-

[7]This is justified because taking into account the q dependence leads to minor changes for low and intermediate energies and momenta, where this effective ph-ph interaction should be used.

[8]Note that q^0/M is of the order $|\vec{q}|^2/M^2$.

[9]Keeping up to next-to-leading terms in the p/M expansion.

[10]The functions U_N and U_Δ are defined in Eqs. (2.9) and (3.4) of Ref. [35], respectively. Besides, note that in a symmetric nuclear medium $U_N=2\overline{U}+$ backward propagating ph excitation. For positive values of q^0 the backward propagating ph excitation has no imaginary part, and for QE kinematics U_Δ is also real.

rated in U_N and U_Δ and then the same interaction strengths V_l and V_t are used for ph and Δh excitations [5,6]. Taking $\vec{q}$ in the z direction, Eq. (40) implies that the axial vector contribution to the transverse (xx,yy) and longitudinal (zz) components of the hadronic tensor get renormalized by different factors $1/|1-U(q,k_F)V_t(q)|^2$ versus $1/|1-U(q,k_F)V_l(q)|^2$.

Let us pay now attention to the term $\mathcal{A}_2$ in Eq. (38), which comes from the interference between the $-g^{\mu i}\sigma^j\tau_+/2$ and $\tau_+ g^{\mu 0}[\vec{\sigma}\cdot(\vec{p}+\vec{p}')]/4M$ operators in Eq. (37). The consideration of the full RPA series leads now to the substitution[11]

$$8M^2\frac{q^0}{|\vec{q}|}G_A^2\,\mathrm{Im}\,\overline{U}(q,k_F^n,k_F^p)\to 8M^2\frac{q^0}{|\vec{q}|}G_A^2\frac{\mathrm{Im}\,\overline{U}(q,k_F^n,k_F^p)}{|1-U(q,k_F)V_l(q)|^2} \tag{41}$$

in the $0z$ and $z0$ components of the hadronic tensor $W^{\mu\nu}$.

Keeping track of the responsible operators, we have examined and renormalized all different contributions to the CC nucleon tensor $A^{\mu\nu}$, by summing up the RPA series depicted in Fig. 3. The 00, $0z$, zz, xx, and xy components of the RPA renormalized CC nucleon tensor[12] can be found in Appendix A. As mentioned above, since the ph(Δh)-ph(Δh) effective interaction is nonrelativistic, we have computed polarization effects only for the leading and next-to-leading terms in the p/M expansion. Thus, order $O(k_F\vec{p}^2/M^2, k_F\vec{p}'^2/M^2, k_F q^0/M)$ has been neglected in the formulae of Appendix A. We have made an exception to the above rule, and since μ_V could be relatively large, we have taken $\mu_V F_2^V|\vec{q}|/M$ to be of order $O(0)$ in the p/M expansion. Finally, we should stress that the scalar-isovector term of the effective interaction (f') cannot produce Δh excitations, and therefore, when this term is involved in the RPA renormalization, only the nucleon Lindhard function (U_N) appears [see coefficient $\mathbf{C_N}$ in Eq. (A9)].

To finish this section we will discuss the differences between the medium polarization scheme presented here and that undertaken in Refs. [12,21]. There is an obvious difference, since in these latter references the scalar-isovector term (f') of the ph-ph effective interaction was not taken into account. In addition, there are some differences concerning the tensorial treatment of the RPA response function. In the framework presented in this work we first evaluate the 1p1h hadronic tensor and all sorts of polarization (RPA) corrections to the different components of this tensor. In a second step we contract it with the leptonic tensor and obtain the differential cross section.[13] The RPA corrections do not depend only on the different terms of the nucleon currents, but also on the particular component of the hadronic tensor that is being renormalized. Thus, as it is obvious, the RPA corrections, in general, are different for each of the terms $[(F_1^V)^2, (F_2^V)^2, F_1^V F_2^V, G_A^2, G_P^2, G_A G_P, F_1^V G_A$, and $F_2^V G_A$, with $G_P = 2MG_A/(m_\pi^2 - q^2)]$ appearing in the CC nucleon tensor. Besides, for a fixed term, the polarization effects also depend on the tensor component. Indeed, we have already mentioned this fact in the discussion of Eq. (40), where we saw that the axial vector contribution to the transverse (xx,yy) and the longitudinal (zz) components of the hadronic tensor get renormalized by different factors.

In the works of Refs. [12,21] the 1p1h hadronic tensor, without polarization effects included, is first contracted with the leptonic one. This contraction is denoted as, up to global kinematical factors, $\overline{\Sigma\Sigma}|T|^2$ in those references. In a second step, the authors of Refs. [12,21] study the medium polarization corrections to $\overline{\Sigma\Sigma}|T|^2$. They find different medium corrections for each of the terms of the CC nucleon tensor $[(F_1^V)^2, \ldots, F_2^V G_A]$, as we do. However, for a fixed term, they cannot independently study the effect of the RPA resummation in each of the different tensor components, since they are not dealing with the hadronic tensor itself, but with the contraction of it with the leptonic one. As a matter of example, to account for the RPA corrections to the axial vector-axial vector term, the following substitution is given in Refs. [12,21]:

$$G_A^2\to G_A^2\left(\frac{2}{3|1-U(q,k_F)V_t(q)|^2}+\frac{1}{3|1-U(q,k_F)V_l(q)|^2}\right). \tag{42}$$

The above substitution can be recovered from Eq. (40) by contracting this latter equation with δ_{ij}, and replacing $2\overline{U}\to U$. Thus, Eq. (42) is strictly correct, neglecting terms[14] of order p/M, only for the contribution to $\overline{\Sigma\Sigma}|T|^2$ obtained from the contraction of the hadronic tensor with the $g_{\mu\nu}$ term[15] of the leptonic one. The prescription of Eq. (42) is not correct for those contributions to $\overline{\Sigma\Sigma}|T|^2$ arising from the contraction of the $k'_\mu k_\sigma + k'_\sigma k_\mu$ terms of the leptonic tensor with the axial vector–axial vector contribution of $W^{\mu\nu}$. Note, however, that neglecting the bound muon three-momentum[16] and up to terms of order p/M, Eq. (42) is correct for the study of inclusive muon capture in nuclei, where it was first used by the authors of Refs. [12,21], and it is also reasonable for neutrino-nucleus reactions at low energies, where the RPA effects are more important.

B. Correct energy balance and Coulomb distortion effects

To ensure the correct energy balance in the reaction (2) for finite nuclei, the energy-conserving δ function in Eq. (28) has to be modified [12,21]. The energies $E(\vec{p})$ and $E(\vec{p}+\vec{q})$ in

[11] To evaluate the longitudinal contribution we use $2p_z+q_z=(2\vec{p}+\vec{q})\cdot\vec{q}/|\vec{q}|=q^0\,[2E(\vec{p})+q^0]/|\vec{q}|=2Mq^0/|\vec{q}|+O(\vec{p}^2/M^2, q^0/M)$. Besides, the transverse part of the effective interaction does not contribute since $(\delta_{zk}-\hat{q}_z\hat{q}_k)(2\vec{p}+\vec{q})_k=0$.

[12] These are the needed components to compute the hadronic tensor $W^{\mu\nu}$, when $\vec{q}$ is taken in the z direction.

[13] Note that the differential cross section is determined by the 00, $0z$, zz, xx, and xy components of $W^{\mu\nu}$ through their relation to the $W_{i=1,\ldots,5}$ structure functions. See Eqs. (9) and (10).

[14] Medium renormalization effects are taken into account in these terms by means of the substitution of Eq. (41).

[15] Note that the axial vector-axial vector contribution to W^{00} is order $O(\vec{p}^2/M^2)$.

[16] This is an accurate approximation and we will also make use of it in Sec. V.

the argument of the δ function refer to the LFG of the nucleons in the initial and final nucleus. In the Fermi sea there is no energy gap for the transition from the occupied to the unoccupied states and hence ph excitations can be produced with a small energy, $Q^{\rm LFG}(r)=E_F^p(r)-E_F^n(r)$. However, in actual nuclei there is a minimum excitation energy, $Q=M(A_{Z+1})-M(A_Z)$, needed for the transition to the ground state of the final nucleus. For instance, this Q value is 16.827 MeV for the transition $^{12}{\rm C}_{gs}\to{}^{12}{\rm N}_{gs}$ and the consideration of this energy gap is essential to obtain reasonable cross sections for low-energy neutrinos. We have taken it into account by replacing

$$q^0\to q^0-[Q-Q^{\rm LFG}(r)] \tag{43}$$

in the δ function of the right hand side of Eq. (28).

The second effect that we want to address here is due to the fact that the charged lepton produced in the reaction of Eq. (2) is moving in the Coulomb field of the nucleus described by a charge distribution $\rho_{ch}(r)$. In our scheme, we implement the corrections due to this effect following the semiclassical approximation used in Ref. [21]. Thus, we include a self-energy (Coulomb potential) in the intermediate lepton propagator of the neutrino self-energy depicted in Fig. 1. We approximate this selfenergy inside the LFG by

$$\Sigma_C=2k'^0V_C(r),$$

$$V_C(r)=-4\pi\alpha\left(\frac{1}{r}\int_0^r dr'r'^2\rho_{ch}(r')+\int_r^{+\infty}dr'r'\rho_{ch}(r')\right) \tag{44}$$

with $\alpha=1/137.036$ and the charge distribution, ρ_{ch}, normalized to Z. The evaluation of the imaginary part of the ν self-energy in the medium requires to put the intermediate lepton propagator on the mass shell. Following Cutkosky's rules, and neglecting quadratic corrections in V_C, we find

$$\frac{1}{k'^2-m_l^2-2k'^0V_C(r)+i\epsilon}\to -i\pi\frac{\delta(k'^0-E_l')}{k'^0}\Theta(\hat{E}_l'(r)-m_l), \tag{45}$$

where E_l' is the asymptotical outgoing lepton energy in regions where the Coulomb potential can be neglected, and the local outgoing lepton energy, $\hat{E}_l'(r)$, is defined by energy conservation

$$\hat{E}_l'(r)+V_C(r)=\sqrt{m_l^2+\vec{\mathcal{K}}'^2(r)}+V_C(r)=E_l'. \tag{46}$$

Because of the Coulomb potential, the outgoing lepton three-momentum, $\vec{\mathcal{K}}'$, is not longer conserved, and it becomes a function of r, taking its asymptotical value, $\vec{k}'$, at large distances. Therefore, $\vec{q}$ should also be replaced by a local function: $\vec{q}'(r)=\vec{k}-\vec{\mathcal{K}}'(r)$. Furthermore, from the d^3k' integration in Eq. (14), and considering now the locality of the three-momentum, we get from phase space a correction factor $|\vec{\mathcal{K}}'(r)|\hat{E}_l'(r)/|\vec{k}'|E_l'$. This way of taking into account the Coulomb effects has clear resemblances with what is called "modified effective momentum approximation" in Ref. [36]. The use of a plane-wave approximation in the interaction region is equivalent to the assumption that the Coulomb potential does not change the direction of the particles when they leave the nucleus. It should therefore not strongly alter an outgoing negatively charged lepton wave packet, which asymptotically is spherical, after it leaves the nucleus except by slowing it down and thereby changing the average radial wavelength and amplitude as the wave moves to larger r. As is shown in Ref. [36], for total cross sections this procedure works very accurately for muons down to low energies. For low-energy electrons and positrons it is less accurate, and the use of the Fermi function $F(Z,E_l')$ [37] is widely accepted in the literature. Anyway, Coulomb effects are small and they become relatively sizable only for neutrino-induced reactions near threshold and/or for heavy nuclei.

To summarize the results of Secs. III A and III B, our final expression for the hadronic tensor is given by

$$W^{\mu\nu}(q^0,\vec{q})=-\frac{\cos^2\theta_C}{2M^2}\int_0^\infty drr^2\frac{|\vec{\mathcal{K}}'(r)|\hat{E}_l'(r)}{|\vec{k}'|E_l'}\Theta(\hat{E}_l'(r)-m_l)$$
$$\times\left\{2\Theta(q'^0)\int\frac{d^3p}{(2\pi)^3}\frac{M}{E(\vec{p})}\frac{M}{E(\vec{p}+\vec{q}')}\right.$$
$$\times\Theta(k_F^n(r)-|\vec{p}|)\Theta(|\vec{p}+\vec{q}'|-k_F^p(r))(-\pi)\delta(q'^0$$
$$\left.+E(\vec{p})-E(\vec{p}+\vec{q}'))\,A^{\nu\mu}_{\rm RPA}(p,q')|_{p^0=E(\vec{p})}\right\} \tag{47}$$

with $q'^0=q^0-[Q-Q^{\rm LFG}(r)]$, $\vec{q}'(r)=\vec{k}-\vec{\mathcal{K}}'(r)$, and $A^{\mu\nu}_{\rm RPA}$ given in Appendix A 2.

C. FSI effects

Once a ph excitation is produced by the virtual W boson, the outgoing nucleon can collide many times, thus inducing the emission of other nucleons. The result is a quenching of the QE peak with respect to the simple ph excitation calculation and a spreading of the strength, or widening of the peak. The integrated strength over energies is not much affected though. A distorted wave approximation with an optical (complex) nucleon nucleus potential would remove all these events. However, if we want to evaluate the inclusive (ν_l,l^-) cross section these events should be kept and one must sum over all open final state channels.

In our MBF we will account for the FSI by using nucleon propagators properly dressed with a realistic self-energy in the medium, which depends explicitly on the energy and the momentum [39]. This self-energy leads to nucleon spectral functions in good agreement with accurate microscopic approaches like the ones of Refs. [40,41]. The self-energy of Ref. [39] has a proper energy-momentum dependence plus an imaginary part from the coupling to the 2p2h components, which is equivalent to the use of correlated wave functions, evaluated from realistic NN forces and incorporating the effects of the nucleon force in the nucleon pairs. Thus, we consider the many-body diagram depicted in Fig. 4 (there the dashed lines stand for an NN interaction inside of the nuclear medium [5,39]).

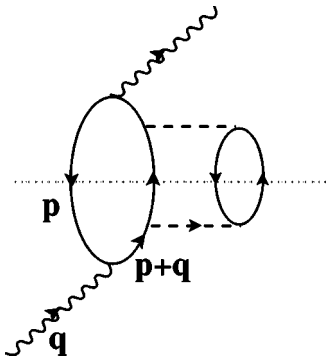

FIG. 4. W^+ self-energy diagram obtained from the first diagram depicted in Fig. 2 by dressing up the nucleon propagator of the particle state in the ph excitation.

However, a word of caution is in order since the imaginary part of this diagram presents a divergency. The reason is that when placing the 2p2h excitation on the mass shell through Cutkosky rules, we still have the square of the nucleon propagator with momentum $p+q$ in the figure. This propagator can be placed on shell for virtual W bosons and we get a divergence.

The divergence is not spurious, in the sense that its meaning is the probability per unit time of absorbing a virtual W^+ by one nucleon times the probability of collision of the final nucleon with other nucleons in the infinite Fermi sea in the lifetime of this nucleon. Since this nucleon is real, its lifetime is infinite and thus the probability is infinite, as well. The problem is physically solved [42] by recalling that the nucleon in the Fermi sea has a self-energy with an imaginary part that gives it a finite lifetime (for collisions). This is taken into account by iterating, in the Dyson equation sense, the nucleon self-energy insertion of Fig. 5 in the nucleon line, hence substituting the particle nucleon propagator, $G(p;\rho)$, in Eq. (20) by a renormalized nucleon propagator, $G_{\rm FSI}(p;\rho)/2M$, including the nucleon self-energy in the medium, $\Sigma(p^0,\vec{p};\rho)$,

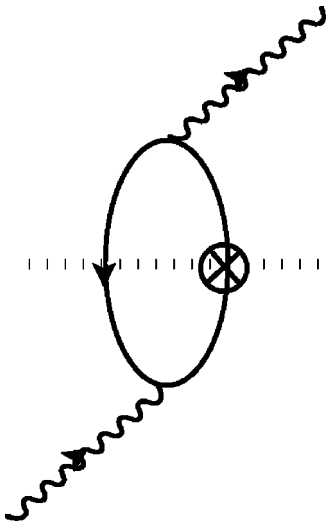

FIG. 5. Insertion of the nucleon self-energy on the nucleon line of the particle state.

$$G_{\rm FSI}(p;\rho)=\frac{1}{p^0-\overline{E}(\vec{p})-\Sigma(p^0,\vec{p};\rho)} \tag{48}$$

with $\overline{E}(\vec{p})=M+\vec{p}^{\,2}/2M$. As mentioned above, we use here the nucleon self-energy model developed in Ref. [39], which led to excellent results in the study of inclusive electron scattering from nuclei [9]. Since the model of Ref. [39] is not Lorentz relativistic and it also considers an isospin symmetric nuclear medium, we will only discuss the FSI effects for nuclei with approximately equal number of protons and neutrons, and using nonrelativistic kinematics for the nucleons (see Appendix C). Thus, we have obtained Eq. (48) from the nonrelativistic reduction of $G(p;\rho)$, in Eq. (20), by including the nucleon self-energy.

Alternatively to the nucleon self-energy language, one can use the spectral function representation

$$G_{\rm FSI}(p;\rho)=\int_{-\infty}^{\mu}\frac{S_h(\omega,\vec{p};\rho)}{p^0-\omega-i\epsilon}d\omega+\int_{\mu}^{\infty}\frac{S_p(\omega,\vec{p};\rho)}{p^0-\omega+i\epsilon}d\omega, \tag{49}$$

where S_h, S_p are the hole and particle spectral functions related to nucleon self-energy Σ by means of

$$S_{p,h}(\omega,\vec{p};\rho)=\mp\frac{1}{\pi}\frac{{\rm Im}\,\Sigma(\omega,\vec{p};\rho)}{[\omega-\overline{E}(\vec{p})-{\rm Re}\,\Sigma(\omega,\vec{p};\rho)]^2+[{\rm Im}\,\Sigma(\omega,\vec{p};\rho)]^2} \tag{50}$$

with $\omega\geqslant\mu$ and $\omega\leqslant\mu$ for S_p and S_h, respectively. The chemical potential μ is determined by

$$\mu=M+\frac{k_F^2}{2M}+{\rm Re}\,\Sigma(\mu,k_F). \tag{51}$$

By means of Eq. (49) we can write the ph propagator or new Lindhard function incorporating the effects of the nucleon self-energy in the medium, and we have for its imaginary part (for positive values of q^0)

$$-{\rm Im}\,\overline{U}_{FSI}(q;k_F)=\frac{\Theta(q^0)}{4\pi^2}\int d^3p\int_{\mu-q^0}^{\mu}d\omega S_h(\omega,\vec{p};\rho)\times S_p(q^0+\omega,\vec{p}+\vec{q};\rho). \tag{52}$$

Comparing the above expression with that of the ordinary imaginary part of the nonrelativistic Lindhard function, Eq. (C3), one realizes that to account for FSI effects in an isospin symmetric nuclear medium of density ρ we should make the following substitution

$$2\Theta(q^0)\int\frac{d^3p}{(2\pi)^3}\Theta(k_F^n(r)-|\vec{p}|)\Theta(|\vec{p}+\vec{q}|-k_F^p(r))(-\pi)$$
$$\times\delta(q^0+\overline{E}(\vec{p})-\overline{E}(\vec{p}+\vec{q}))A^{\nu\mu}(p,q)|_{p^0=\overline{E}(\vec{p})}$$
$$\to-\frac{\Theta(q^0)}{4\pi^2}\int d^3p\int_{\mu-q^0}^{\mu}d\omega S_h(\omega,\vec{p};\rho)$$
$$\times S_p(q^0+\omega,\vec{p}+\vec{q};\rho)A^{\nu\mu}(p,q)|_{p^0=\overline{E}(\vec{p})} \quad (53)$$

in the expression of the hadronic tensor [Eq. (28)]. The d^3p integrations have to be done numerically. Indeed, the integrations are not trivial from the computational point of view, since in some regions the spectral functions behave like δ functions. We use the spectral functions calculated in Ref. [39], but since the imaginary part of the nucleon self-energy for the hole states is much smaller than that of the particle states at intermediate nuclear excitation energies, we make the approximation of setting to zero Im Σ for the hole states. This was found to be a good approximation in [43]. Thus, we take

$$S_h(\omega,\vec{p};\rho)=\delta(\omega-\hat{E}(\vec{p}))\Theta(\mu-\hat{E}(p)), \quad (54)$$

where $\hat{E}(p)$ is the energy associated with a momentum $\vec{p}$ obtained self-consistently by means of the equation

$$\hat{E}(\vec{p})=\overline{E}(\vec{p})+\mathrm{Re}\,\Sigma(\hat{E}(\vec{p}),\vec{p};\rho). \quad (55)$$

It must be stressed that it is important to keep the real part of Σ in the hole states when renormalizing the particle states because there are terms in the nucleon self-energy largely independent of the momentum and that cancel in the ph propagator, where the two self-energies subtract.

On top of the FSI corrections examined here, one should also take into account the nuclear corrections studied previously in Secs. III A and III B.

IV. CC ANTINEUTRINO-INDUCED NUCLEAR REACTIONS

The cross section for the antineutrino-induced nuclear reaction

$$\overline{\nu_l}(k)+A_Z\to l^+(k')+X \quad (56)$$

is easily obtained from the expressions given in Secs. II and III with the following modifications:

(a) Changing the sign of the parity-violating terms, proportional to W_3, in the differential cross section, Eq. (10).

(b) Replacing the W^+ self-energy in the medium, $\Pi_W^{\mu\nu}$, by that of the W^- boson ($\overline{\Pi}_W^{\mu\nu}$). This is achieved by exchanging the role of protons and neutrons in all formulas $\overline{\Pi}_W^{\mu\nu}(\rho_p(r),\rho_n(r))=\Pi_W^{\mu\nu}(\rho_n(r),\rho_p(r))$.

(c) Changing the sign of V_C, which turns out to be repulsive for positive charged outgoing leptons.

(d) Correcting the LFG energy balance with the difference $\overline{Q}-\overline{Q}^{\mathrm{LFG}}(r)$, with $\overline{Q}=M(A_{Z-1})-M(A_Z)$ and $\overline{Q}^{\mathrm{LFG}}(r)=E_F^n(r)-E_F^p(r)$.

V. INCLUSIVE MUON CAPTURE IN NUCLEI

In this section we study the μ-atom inclusive decay, that is to say, the reaction

$$(A_Z-\mu^-)^{1s}_{\mathrm{bound}}\to\nu_\mu(k)+X. \quad (57)$$

It is obvious that the dynamics that governs this process is related to that of antineutrino- [Eq. (56)] and neutrino- [Eq. (2)] induced nuclear processes, but a distinctive feature is that the nuclear excitation energies involved in the μ-atom decay are extremely low (smaller than $\approx$20 MeV). In this energy regime one might expect important inaccuracies in the LFG description of the nucleus. However and due to the inclusive character of the process, we will see that our MBF leads to reasonable results, with discrepancies of the order of 10–15 % at most, with RPA effects as large as a factor of 2. We should emphasize that similar conclusions were achieved in the works of Ref. [12], which also use a LFG picture of the nucleus.

The evaluation of the decay width for finite nuclei proceeds in two steps. In the first one we evaluate the spin-averaged decay width for a muon at rest[17] in a Fermi sea of protons and neutrons with $N\neq Z$. In this first step, the strong renormalization effects (RPA) will be also taken into account and thus we will end up with a decay width $\hat{\Gamma}$, which will be a function of the proton and neutron densities. In the second step, we use the LDA to go to finite nuclei and evaluate

$$\Gamma=\int d^3r|\phi_{1s}(\vec{r})|^2\hat{\Gamma}(\rho_p(r),\rho_n(r)), \quad (58)$$

where $\phi_{1s}(\vec{r})$ is the muon wave function in the 1s state from where the capture takes place. It has been obtained by solving the Schrödinger equation with a Coulomb interaction, taking account of the finite size of the nucleus and vacuum polarization [38]. Equation (58) amounts to saying that every bit of the muon, given by the probability $|\phi_{1s}(\vec{r})|^2d^3r$, is surrounded by a Fermi sea of densities $\rho_p(r)$, $\rho_n(r)$. The LDA assumes a zero range of the interaction, or equivalently no dependence on $\vec{q}$. The $\vec{q}$ dependence of the interaction is extremely weak for the μ-atom decay process, and thus the LDA prescription becomes highly accurate [12].

The spin-averaged muon decay width, in an infinite nuclear matter of densities $\rho_p(r)$ and $\rho_n(r)$, is related to the imaginary part of the self-energy (see Fig. 6), $\Sigma_\mu^r(\rho_p(r),\rho_n(r))$, of a muon at rest and spin r in the medium by

$$\hat{\Gamma}(\rho_p(r),\rho_n(r))=-\frac{1}{m_\mu}\mathrm{Im}\,\Sigma_\mu(\rho_p(r),\rho_n(r)),\quad \Sigma_\mu=\frac{1}{2}\sum_r\Sigma_\mu^r. \quad (59)$$

To evaluate the imaginary part of the self-energy associated with the diagram of Fig. 6, the intermediate states are placed on shell in the integration over the internal variables. These states are those crossed by the dash-dotted line in Fig. 6. The

[17] In what follows, we will neglect the three-momentum of the bound muon.

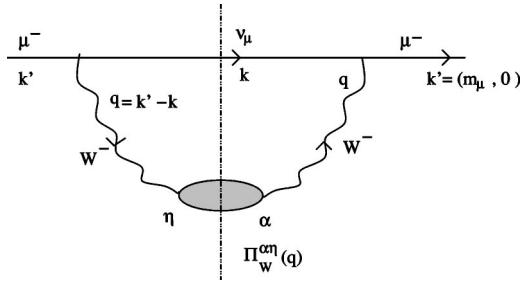

FIG. 6. Diagrammatic representation of the muon (at rest) self-energy in nuclear matter.

evaluation of the μ self-energy is almost identical to that of a neutrino in Fig. 1, and thus we obtain[18] from Eq. (14),

$$\hat{\Gamma}(\rho_p(r),\rho_n(r)) = -\frac{1}{m_\mu}\frac{4G}{\sqrt{2}M_W^2}\int \frac{d^3k}{(2\pi)^3}\frac{\Theta(q^0)}{2|\vec{k}|} \times \mathrm{Im}\{\overline{\Pi}_W^{\mu\eta}(q;\rho_p(r),\rho_n(r))L_{\mu\eta}\} \quad (60)$$

with $q^0 = m_\mu - |\vec{k}|$ and $|\vec{q}| = |\vec{k}|$. For kinematical reasons, only the QE part of the W^- self-energy will contribute to the muon decay width and thus we find

$$\hat{\Gamma}(\rho_p(r),\rho_n(r)) = \frac{G^2\cos^2\theta_C}{m_\mu}\int \frac{d^3k}{(2\pi)^3}\frac{1}{2|\vec{k}|}L_{\mu\eta}\mathcal{T}^{\mu\eta}(q;\rho_p,\rho_n)$$
$$= \frac{G^2\cos^2\theta_C}{2\pi^2}\int_0^{+\infty}\vec{k}^2\Big(-t_1+\frac{t_2}{2}+|\vec{k}|t_3+\frac{m_\mu^2}{2}t_4 + m_\mu t_5\Big)d|\vec{k}|, \quad (61)$$

where the tensor $\mathcal{T}^{\mu\nu}$ is defined as

$$\mathcal{T}^{\mu\nu}(q;\rho_p,\rho_n) = -\frac{1}{4M^2}\Bigg\{2\Theta(q^0)\int\frac{d^3p}{(2\pi)^3}\frac{M}{E(\vec{p})}\frac{M}{E(\vec{p}+\vec{q})}\Theta(k_F^p(r) - |\vec{p}|)\Theta(|\vec{p}+\vec{q}| - k_F^n(r)) \times(-\pi)\delta(q^0+E(\vec{p})-E(\vec{p}+\vec{q}))A^{\mu\nu}_{\mathrm{RPA}}(p,q)|_{p^0=E(\vec{p})}\Bigg\}$$
$$\equiv t_1 g^{\mu\nu} + t_2 l^\mu l^\nu + i t_3 \epsilon^{\mu\nu\alpha\beta} l_\alpha q_\beta + t_4 q^\mu q^\nu + t_5(l^\mu q^\nu + l^\nu q^\mu) \text{ with } l^\mu = (1,\vec{0}). \quad (62)$$

The similitude of the above equation with Eq. (28) is clear. As in this latter case, the d^3p integrations in Eq. (62) can be done analytically (see Appendix B) and all of them are determined by the imaginary part of the relativistic isospin asymmetric Lindhard function, $\overline{U_R}(q,k_F^n,k_F^p)$. For a nonrelativistic Fermi gas, the decay width is easily obtained from Eq. (62) by replacing the factors $M/E(\vec{p})$ and $M/E(\vec{p}+\vec{q})$ by one. Analytical expressions can be now found in Appendix C. FSI effects can be also taken into account by performing the substitution of Eq. (53).

Thus, both the muon decay process in the medium and the electroweak inclusive nuclear reactions $\nu_l(k)+A_Z \to l^-(k')+X$ in the QE regime are sensitive to the same physical features, $W^\pm pn$ vertex, and RPA and FSI effects. However, in the muon-atom decay only very small nuclear excitation energies are explored, 0–25 MeV, while in the latter processes higher nuclear excitation energies can be tested by varying the incoming neutrino momentum.

The 1*s* muon binding energy, $B_\mu^{1s} > 0$, can be taken into account, by replacing $m_\mu \to \hat{m}_\mu = m_\mu - B_\mu^{1s}$. This replacement leads to extremely small (significant) changes for light (heavy) nuclei, where B_μ^{1s} is of the order of 0.1 MeV (10 MeV) (see Table I).

Finally, the correct energy balance in the decay can be enforced in the LFG by replacing

$$q^0 \to q^0 - [\overline{Q} - \overline{Q}^{\mathrm{LFG}}(r)] = \hat{m}_\mu - |\vec{k}| - [\overline{Q} - \overline{Q}^{\mathrm{LFG}}(r)] \quad (63)$$

in Eqs. (61) and (62).

VI. RESULTS

Firstly, we compile in Table I the input used for the different nuclei studied in this work. Nuclear masses and charge densities are taken from Refs. [44,45], respectively. For each nucleus, we take the neutron matter density approximately equal (but normalized to *N*) to the charge density, though we consider small changes, inspired by Hartree-Fock calculations with the density-matrix expansion [46] and corroborated by pionic atom data [47]. However, charge (neutron) matter densities do not correspond to proton (neutron) point-like densities because of the finite size of the nucleon. This is taken into account by following the procedure outlined in Sec. II of Ref. [47] [see Eqs. (12–14) of this reference].

A. Inclusive neutrino reactions at low energies

In this section we present results obtained by using non-relativistic kinematics for the nucleons. We do not include FSI effects, since in Sec. III C we made the approximation of setting to zero Im Σ for the hole states. For low nuclear excitation energies ($\leqslant$60), this approximation is not justified, because the imaginary part of the self-energy of particle and hole states are comparable [39]. The inclusion of FSI effects would lead to a quenching of the QE peak of the bare ph calculation, and a spreading of the strength [4,28,29,48,49]. However, FSI effects on integrated quantities are small. From the results of the next section we estimate in $\sim$5–10 % the theoretical error of the integrated cross sections and total muon capture rates presented in this section.

The processes studied in this section explore quite low nuclear excitation energies ($\leqslant$25–30 MeV), and hence one might expect that a proper finite nuclei treatment could be in

[18] There is a factor 1/2 of difference coming from the averaged over initial spins of the muon, besides the W^- self-energy arises since the negative muon decay process is related to the antineutrino-induced process, and the contribution of parity-violating terms flips sign.

TABLE I. Charge (R_p, a), neutron matter (R_n, a) density parameters, $Q, \overline{Q}$ values and negative muon binding energies for different nuclei. For carbon and oxygen we use a modified harmonic oscillator (MHO) density, $\rho(r)=\rho_0[1+a(r/R)^2]\exp[-(r/R)^2]$, while for the rest of the nuclei, a two-parameter Fermi distribution, $\rho(r)=\rho_0/\{1+\exp[(r-R)/a]\}$, was used.

Nucleus	R_p (fm)	R_n (fm)	a (fm)[a]	Q [MeV]	$\overline{Q}$ [MeV]	B_μ^{1s} [MeV]
^{12}C	1.692	1.692	1.082	16.827	13.880	0.100
^{16}O	1.833	1.833	1.544	14.906	10.931	0.178
^{18}O	1.881	1.975	1.544	1.144	14.413	0.178
^{23}Na	2.773	2.81	0.54	3.546	4.887	0.336
^{40}Ca	3.51	3.43	0.563	13.809	1.822	1.064
^{44}Ca	3.573	3.714	0.563	3.142	6.170	1.063
^{75}As	4.492	4.64	0.58	0.353	1.688	2.624
^{112}Cd	5.38	5.58	0.58	2.075	4.462	4.861
^{208}Pb	6.624	6.890	0.549	2.368	5.512	10.510

[a]The parameter a is dimensionless for the MHO density form.

order. Indeed, these processes are sensitive to the excitation of giant resonances [16,18,25,27]. As mentioned in the Introduction, our purpose is to describe the interaction of neutrinos and antineutrinos with nuclei at higher energies (nuclear excitation energies of the order of 100–600 MeV) of interest for future neutrino oscillation experiments. However, our model provides a good description of the low-energy inclusive measurements analyzed in this subsection. RPA correlations play an essential role and lead to reductions as large as a factor of 2. We should remind the reader that the effective interaction appearing in the RPA series was fitted in Ref. [33] to giant resonances, and thus our approach incorporates the mechanism that produces those resonances in finite nuclei.

At low energies, finite nuclei effects are expected to be sizable for outgoing lepton energy distributions. There exist discrete and resonance state peaks, and the continuum distribution significantly differs from the LFG one. However, the integrated strength over energies, including the discrete state and resonance contributions, remains practically unchanged, which explains the success of our model to describe integrated-inclusive magnitudes. A clear example of this can be found in Ref. [48] where the inclusive decay width of muonic atoms by using a shell model with final neutron states lying both in the continuum and in the discrete spectrum are calculated. The results are compared with those obtained from a LFG model. Both models[19] are in quite good agreement within a few percent when the shell model density is used in the LFG calculation. Being an integrated, inclusive observable, the total capture width is quite independent of the fine details of the nuclear wave functions. Similar conclusions were reached in the study of the radiative pion capture in nuclei, $(A_Z-\pi^-)_{\rm bound}\to\gamma+X$, performed in Ref. [49]. There, the predictions of a continuum shell model were also extensively compared to those deduced from a LFG picture of the nucleus. The differences found, among the integrated decay widths predicted by both approaches, were, at most, of the order of 4% (see Table 5 of first entry in Ref. [49]).

1. The inclusive reactions ^{12}C$(\nu_\mu,\mu^-)X$ and ^{12}C$(\nu_e,e^-)X$ near threshold

In order to compare with the experimental measurements we calculate flux-averaged cross sections

$$\overline{\sigma}=\frac{1}{\mathcal{N}}\int_{E_\nu^{\rm min}}^{E_\nu^{\rm max}} dE_\nu \sigma(E_\nu) W(E_\nu), \quad \mathcal{N}=\int_{E_\nu^{\rm min}}^{E_\nu^{\rm max}} W(E_\nu) dE_\nu, \tag{64}$$

In the LSND experiment at Los Alamos, the inclusive ^{12}C$(\nu_\mu,\mu^-)X$ cross section was measured using a pion decay in-flight ν_μ beam, with energies ranging from zero to 300 MeV, and a large liquid scillantor detector [50–52]. The muon neutrino spectrum, $W(E_\nu)$, in taken from Ref. [50] and it is plotted in the left bottom panel of Fig. 7. We fix $E_\nu^{\rm min}$ and $E_\nu^{\rm max}$ to 123.1 and 300 MeV, respectively. The electron neutrino beams used in experiments (LAMPF, KARMEN, etc.) have relatively low energies. Such neutrinos do not constitute a monochromatic beam, and their spectrum[20] is plotted in the right bottom panel of Fig 7. The bare ph strength spreading due to the FSI might affect the inclusive, flux-averaged cross section because of the energy variations in the neutrino flux. As an illustration, if some of the strength is shifted to higher energies then some of the low-energy neutrinos will not be able to excite it, compared with the case when the strength is not spread out. Of course these effects are not very large, because some strength is also moved to lower energies and compensates this. These uncertainties

[19]For simplicity in the calculations of Ref. [48], RPA effects are not considered and the static form of the nucleon CC current is employed.

[20]It is approximately described by the Michel distribution

$$W(E_\nu)\propto E_\nu^2(E_\nu^{\rm max}-E_\nu),\ E_\nu^{\rm max}=\frac{m_\mu^2-m_e^2}{2m_\mu},\ E_\nu^{\rm min}=0. \tag{65}$$

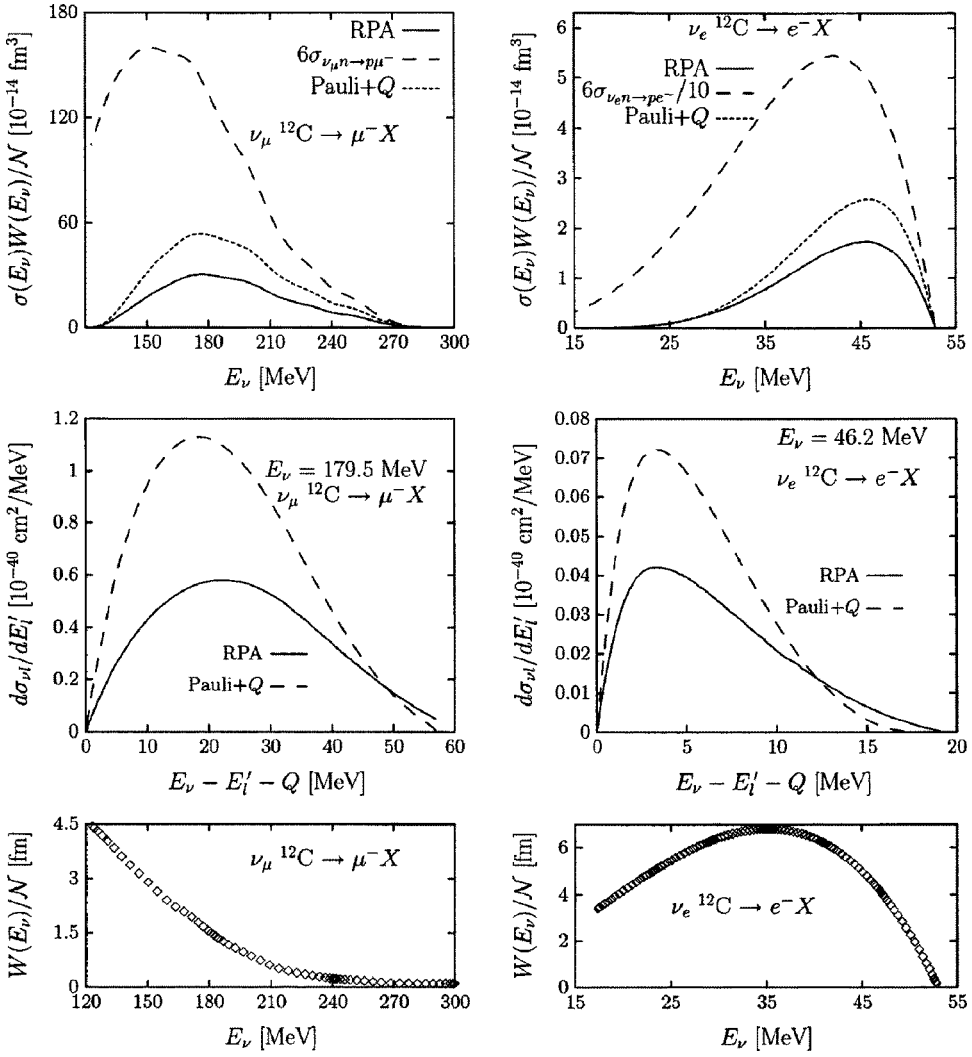

FIG. 7. Predictions for the LSND measurement of the ^{12}C $(\nu_\mu,\mu^-)X$ reaction (left panels) and the ^{12}C $(\nu_e,e^-)X$ reaction near threshold (right panels). Results have been obtained by using nonrelativistic kinematics for the nucleons and without FSI. Top: ν_μ and ν_e cross sections multiplied by the neutrino fluxes, as a function of the neutrino energy. In addition to the RPA calculation (solid line), we show results without RPA correlations and Coulomb corrections (dotted line), and also (dashed line) the low-density limit of Eq. (31). Middle: Differential muon and electron neutrino cross sections at $E_{\nu_\mu}=179.5$ MeV (left) and $E_{\nu_e}=46.2$ MeV (right), as a function of the energy transfer. Bottom: Neutrino spectra from Ref. [50] (left) and Eq. (65) (right).

contribute to the $\sim 5-10\,\%$ theoretical error mentioned above.

Our results for the $^{12}\mathrm{C}(\nu_\mu,\mu^-)X$ and $^{12}\mathrm{C}(\nu_e,e^-)X$ reactions near threshold are presented in Fig. 7 and Table II. As can be seen in the table, the agreement with data is remarkable. Nuclear effects turn out to be essential, and thus the simple prescription of multiplying by a factor of 6 (the number of neutrons of ^{12}C) the free space $\nu_l n\to p l^-$ cross section overestimates the flux-averaged cross sections by a factor of 5 and of 40 for the muon and electron neutrino-induced reactions, respectively. The inclusion of Pauli blocking and the use of the correct energy balance in the reaction lead to much better results, but the cross sections are still badly overestimated. Only once RPA and Coulomb corrections are included a good description of data is achieved. RPA correlations reduce the flux-averaged cross sections by about a factor of 2, while Coulomb distortion significantly enhances them, in particular for the electron neutrino reaction where this enhancement is of about 30%.

In Table II, a few selected theoretical calculations [large basis shell model (SM) results of Refs. [15,27] and the continuum RPA (CRPA) ones from Ref. [18]] are also quoted. Our approach might look simplified with respect to the ones just mentioned, but in fact it is also an RPA approach built up from single-particle states of an uncorrelated Fermi sea. This method in practice is a very accurate tool when the excitation

TABLE II. Experimental and theoretical flux averaged $^{12}\mathrm{C}(\nu_\mu,\mu^-)X$ and $^{12}\mathrm{C}(\nu_e,e^-)X$ cross sections in 10^{-40} cm^2 units. We label our predictions as in Fig. 7. We also quote results from other calculations (see text for details).

	LDT	Pauli+Q	RPA	SM [15]	SM [27]	CRPA [18]	Exp.		
							LSND'95 [50]	LSND'97 [51]	LSND'02 [52]
$\overline{\sigma}(\nu_\mu,\mu^-)$	66.1	20.7	11.9	13.2	15.2	19.2	$8.3\pm0.7\pm1.6$	$11.2\pm0.3\pm1.8$	$10.6\pm0.3\pm1.8$
							KARMEN [53]	LSND [54]	LAMPF [55]
$\overline{\sigma}(\nu_e,e^-)$	5.97	0.19	0.14	0.12	0.16	0.15	$0.15\pm0.01\pm0.01$	$0.15\pm0.01\pm0.01$	0.141 ± 0.023

TABLE III. Experimental and theoretical total muon capture widths for different nuclei. Data are taken from Ref. [56], and when more than one measurement is quoted in Ref. [56], we use a weighted average: $\bar{\Gamma}/\sigma^2=\Sigma_i\Gamma_i/\sigma_i^2$, with $1/\sigma^2=\Sigma_i(1/\sigma_i^2)$. Theoretical results have been obtained by using nonrelativistic kinematics for the nucleons (Appendix C). To illustrate the role played by the RPA correlations, we quote two different theoretical results: (i) Pauli+$\bar{Q}$ obtained from Eq. (62) without including FSI effects and RPA correlations [i.e., replacing $A^{\mu\nu}_{\rm RPA}$ by $A^{\mu\nu}$ in Eq. (62)], but taking into account the value of $\bar{Q}$; (ii) the full calculation, including all nuclear effects with the exception of FSI, presented in Sec. V, and denoted as RPA. Finally, in the last column we show the relative discrepancies existing between the theoretical predictions given in the third column and data.

	Pauli+$\bar{Q}$ (10^4 s^{-1})	RPA (10^4 s^{-1})	Exp. (10^4 s^{-1})	$(\Gamma^{\rm exp}-\Gamma^{\rm th})/\Gamma^{\rm exp}$
^{12}C	5.42	3.21	3.78±0.03	0.15
^{16}O	17.56	10.41	10.24±0.06	−0.02
^{18}O	11.94	7.77	8.80±0.15	0.12
^{23}Na	58.38	35.03	37.73±0.14	0.07
^{40}Ca	465.5	257.9	252.5±0.6	−0.02
^{44}Ca	318	189	179±4	−0.06
^{75}As	1148	679	609±4	−0.11
^{112}Cd	1825	1078	1061±9	−0.02
^{208}Pb	1939	1310	1311±8	0.00

energy is sufficiently large such that relatively many states contribute to the process. Obviously, because of its nature, the method only applies to inclusive processes and it is not meant to evaluate transitions to discrete states. The adaptation of the method to finite nuclei via the LDA has proved to be a rather precise technique to deal with inclusive photonuclear reactions [3] and response functions in electron scattering [4]. The effective ph(Δh)-ph(Δh) interaction used in the RPA series has been successfully employed in different processes [3,4,6]. There are two distinctive features of this interaction in the $S=T=1$ channel, which are not incorporated in most of the finite nuclei approaches: (i) it incorporates explicit pion and ρ exchanges and thus the force in this channel is split into longitudinal and transverse parts, and (ii) it includes resonance Δ degrees of freedom. The inclusion of Δh components in the RPA series reduces the LSND flux-averaged ^{12}C $(\nu_\mu,\mu^-)X$ cross section by about a 15%, while the reduction factor is about 4 times smaller for the electron neutrino reaction, because in this latter case, the larger contributions to the flux-averaged ^{12}C$(\nu_e,e^-)X$ cross section comes from very low ($\leqslant$20 MeV) nuclear excitation energies (see Fig. 7). In addition, a correct tensorial treatment of the RPA hadronic tensor is also important, and it explains the bulk of the existing differences between our results and those obtained in Ref. [21] (see Sec. III A for details). As a matter of example, in Ref. [21] a value of $(16.7\pm1.4)\times10^{-40}$ cm^2 is predicted for the LSND flux-averaged ^{12}C$(\nu_\mu,\mu^-)X$ cross section. This value is about 40% higher than our result, despite of using quite similar ph(Δh)-ph(Δh) effective interactions. Differences are significantly smaller for the electron neutrino flux-averaged cross section, since this reaction is sensitive to quite lower energies.

In the middle panels of Fig. 7, we plot the outgoing lepton energy distribution for an incoming neutrino energy near the maximum of $\sigma(E_\nu)W(E_\nu)$ (top panels). We see in these plots the range of energies transferred $(E_\nu-E_l'-Q)$ to the daughter nucleus: 25–30 MeV for the muon neutrino reaction and less than 10 MeV for the electron neutrino process. Finite nuclei distributions will present some discrete state and narrow resonance peaks, but the integrated strength over energies would not be much affected though, as we have already discussed.

2. Total nuclear capture rates for negative muons

After the success in describing the LSND measurement of the reaction ^{12}C$(\nu_\mu,\mu^-)X$ near threshold, it seems natural to further test our model by studying the closely related process of inclusive muon capture in ^{12}C. Furthermore, and since there are abundant and accurate measurements of nuclear inclusive muon capture rates through the whole periodic table, we have also calculated muon capture widths for a few selected nuclei, which will be also studied below in Sec. VI B. Our results are compiled in Table III. Data are quite accurate, with precisions smaller than 1%, quite far from the theoretical uncertainties of any existing model. Medium polarization effects (RPA correlations), once more, are essential to describe the data, as was already shown in Ref. [12]. Despite the huge range of variation of the capture widths,[21] the agreement to data is quite good for all studied nuclei, with discrepancies of about 15% at most. It is precisely for ^{12}C, where we find the greatest discrepancy with experiment. Nevertheless, our model provides one of the best existing combined description of the inclusive muon capture in ^{12}C and the LSND measurement of the reaction ^{12}C$(\nu_\mu,\mu^-)X$ near threshold [18].

Finally, in Fig. 8 we show the outgoing ν_μ energy distribution from muon capture in ^{12}C, which ranges from

[21]Note, $\Gamma^{\rm exp}$ varies from about 4×10^4 s^{-1} in ^{12}C to 1300 $\times10^4$ s^{-1} in ^{208}Pb.

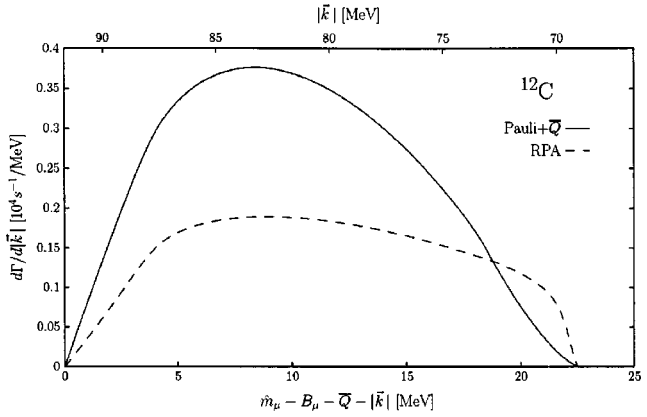

FIG. 8. Inclusive muon capture differential width from ^{12}C, as a function of the outgoing neutrino energy (top axis) and of the energy transfer (bottom axis). Nonrelativistic kinematics has been used for the nucleons. The two calculations are labeled as in Table III.

70 to 90 MeV. The energy transferred to the daughter nucleus (^{12}B) ranges from 0 to 20 MeV. We also show in the figure the medium polarization effect on the differential decay rate. As already mentioned, the shape of the curves in Fig. 8 will significantly change if a proper finite nuclei treatment is carried out, with the appearance of narrow peaks, but providing similar values for the integrated widths [48].

B. Inclusive QE neutrino and antineutrino reactions at intermediate energies

In this section we will present results on muon and electron neutrino- and antineutrino-induced reactions in several nuclei for intermediate energies, where the predictions of the model developed in this work are reliable, not only for integrated cross sections, as in the preceding section, but also for differential cross sections. We will present results for incoming neutrino energies within the interval 150–400 (250–500) MeV for electron (muon) species. The use of relativistic kinematics for the nucleons leads to moderate reductions of both neutrino and antineutrino cross sections, ranging these reductions in the interval 4–9 %, at the intermediate energies considered in this work. Such corrections do not depend significantly on the considered nucleus.

In Fig. 9, the effects of RPA and Coulomb corrections are studied as a function of the incoming neutrino/antineutrino energy. These corrections are important (20–60 %), both for neutrino and antineutrino reactions, in the whole range of considered energies. RPA correlations reduce the cross sections, and we see large effects, specially at lower energies. The RPA reductions become smaller as the energy increases. Nevertheless for the higher energies considered (500 and 400 MeV for muon and electron neutrino reactions, respectively) we still find suppressions of about 20–30 %. Coulomb distortion of the outgoing charged lepton enhances (reduces) the cross sections for neutrino (antineutrino) processes. Coulomb effects decrease with energy. For antineutrino reactions, the combined effect of RPA and Coulomb corrections have a moderated dependence on A and Z. Coulomb corrections reduce the outgoing positive charged lepton effective momentum inside of the nuclear medium. Thus, the phase space correction factor $|\vec{K}'(r)|\hat{E}'_l(r)/|\vec{k}'|E'_l$ is smaller than one and the cross section gets smaller. This effect, obviously grows with Z. On the other hand, the RPA suppression decreases when the lepton effective momentum increases and it grows with A. The combined effect explains the nuclear dependence found in the antineutrino plots. At the higher-energy end the A dependence becomes milder, since Coulomb distortion becomes less important. In the case of neutrinos, the increase of the cross section due to Coulomb cancels out partially with the RPA reduction. Finally, the existing differences between electron and muon neutrino/antineutrino plots are due to the different momenta of an electron and a muon with the same energy.

In Fig. 10, we show electron and muon neutrino and antineutrino inclusive QE cross sections and ratios for different

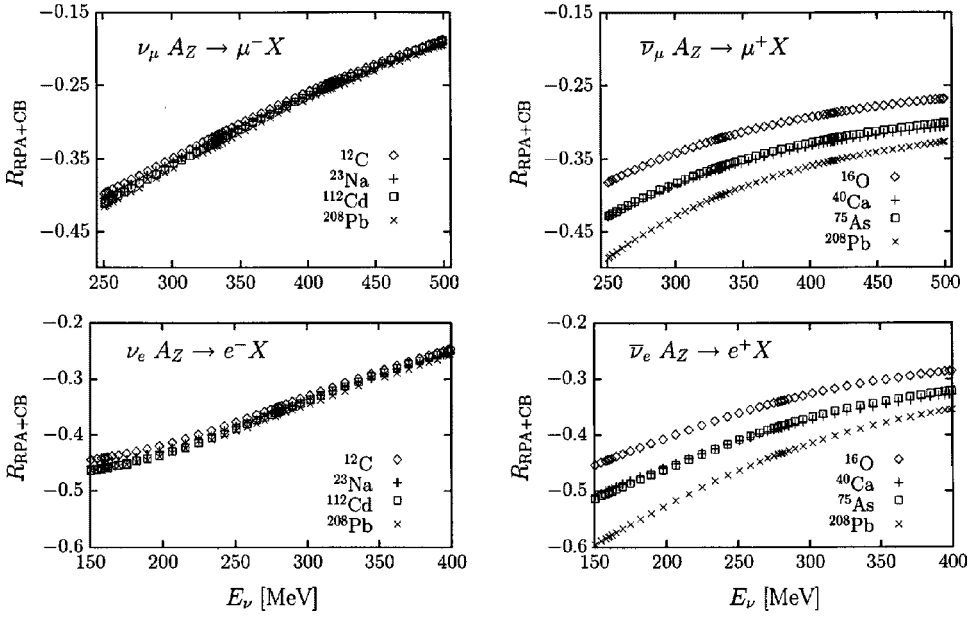

FIG. 9. RPA and Coulomb (CB) corrections to electron and muon neutrino and antineutrino QE cross sections for different nuclei, as a function of the neutrino energy. A relativistic treatment of the nucleons is undertaken and FSI effects are not considered. $R_{\mathrm{RPA+CB}}$ is defined as $(\sigma_{\mathrm{RPA+CB}} - \sigma_0)/\sigma_0$, where σ_0 does not include RPA and Coulomb corrections, while $\sigma_{\mathrm{RPA+CB}}$ includes these nuclear effects.

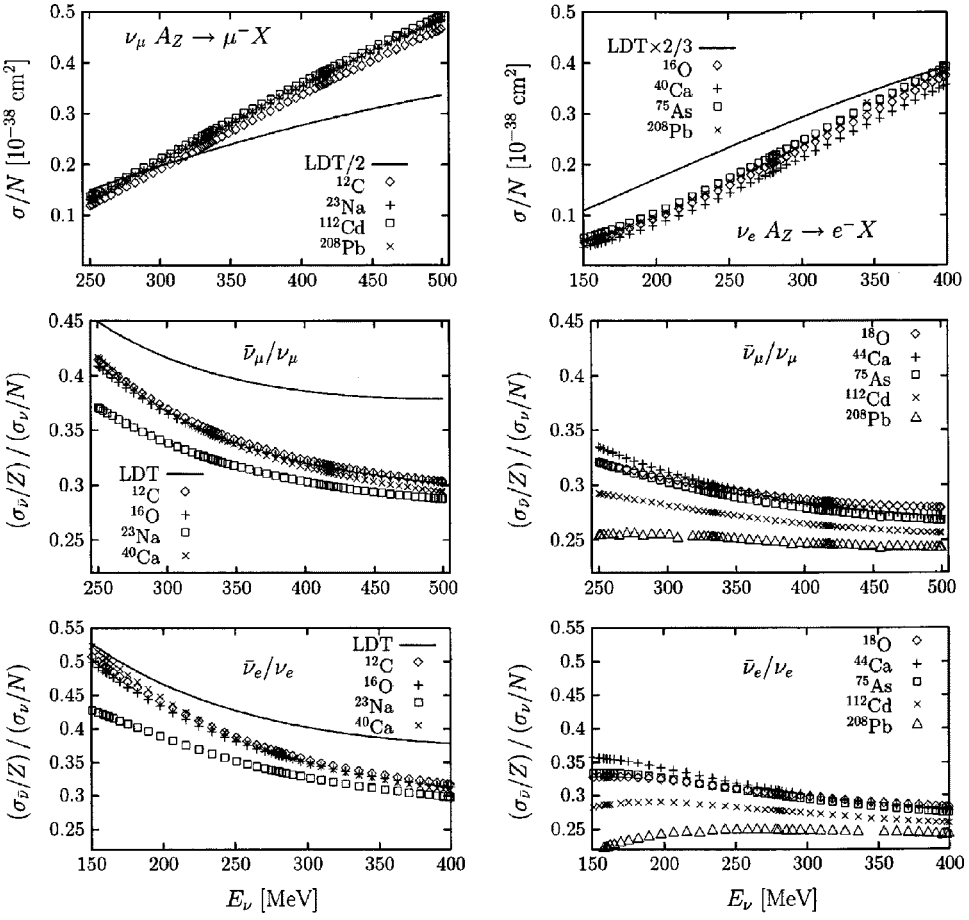

FIG. 10. Electron and muon neutrino and antineutrino inclusive QE cross sections and ratios for different nuclei, at intermediate energies. Results have been obtained with the full model without FSI, and using relativistic kinematics for the nucleons. For comparison we also show results obtained in the free space [low-density limit, LDT, Eq. (31)].

nuclei, as a function of the incoming lepton energy. Results have been obtained with the full model presented in Sec. III, including all nuclear effects with the exception of FSI, and using relativistic kinematics for the nucleons. Neutrino cross sections scale with N (number of neutrons) reasonably well, while there exist important departures from a Z (number of protons) scaling rule for antineutrino cross sections. These departures can be easily understood from the discussion of Fig. 9. To better disentangle medium effects, the free space neutrino/antineutrino nucleon cross section multiplied by the number of neutrons or protons is also depicted in the plots.

In Fig. 11 we show muon neutrino and antineutrino inclusive QE differential cross sections as a function of the energy transfer, for different isoscalar nuclei and different incoming lepton energies. We see an approximate A scaling and once more the important role played by the medium polarization effects. Similar results (not shown in the figure) are obtained from electron species.

The double differential cross section $d\sigma/dE_l' d|\vec{q}|$ for the muon neutrino reaction in calcium is shown in Fig. 12. In the top panel, we compare the lepton scattering angle distribution for three different values of the energy transfer. As usual in QE processes, the peaks of the distributions are placed in the vicinity of $|\vec{q}| = \sqrt{2Mq^0}$. In the bottom panel, we show FSI effects on the differential cross section for one of the energies ($E_l' = 228.6$ MeV) studied in the upper panel. We also show the effects of using relativistic kinematics for the nucleons. As anticipated, FSI provides a broadening and a significant reduction of the strength of the QE peak. Nevertheless the $|\vec{q}|$ integrated cross section is only slightly modi-

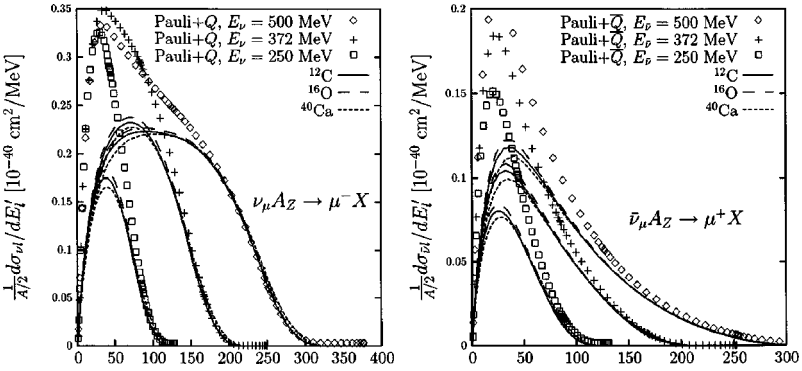

FIG. 11. Muon neutrino and antineutrino relativistic QE differential cross sections from different nuclei and several $\nu_\mu, \bar{\nu}_\mu$ energies. Results, denoted as "Pauli+Q" or "Pauli+$\bar{Q}$" have been obtained in ^{12}C and do not include RPA, FSI, and Coulomb effects, while the rest of the results have been obtained with the full model without FSI.

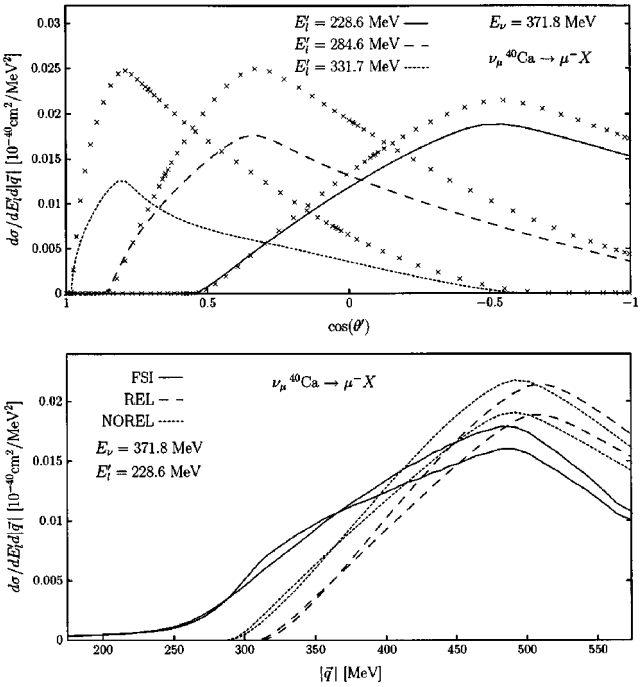

FIG. 12. Muon neutrino differential cross sections in calcium as a function of the lepton scattering angle (top) and of the momentum transfer (bottom). The neutrino energy is 371.8 MeV. Top: Cross sections, without FSI and using relativistic kinematics for the nucleons, at different muon energies. Crosses have been obtained without RPA and Coulomb effects, while the curves have been obtained with the full model (up to FSI effects). Bottom: Cross sections, for a muon energy of 228.6 MeV, obtained by using relativistic (long dashed line REL) and nonrelativistic nucleon kinematics. In this latter case, we present results with (solid line, FSI) and without (short dashed line, NOREL) FSI effects. For the three cases, we also show the effect of taking into account RPA and Coulomb corrections (lower lines at the peak). The areas (in units of 10^{-40} cm^2/MeV) below the curves are 3.50 (REL), 3.87 (NOREL), and 3.77 (FSI) when RPA and Coulomb corrections are not considered, and 3.13 (REL), 3.49 (NOREL), and 3.53 (FSI) when these nuclear effects are taken into account.

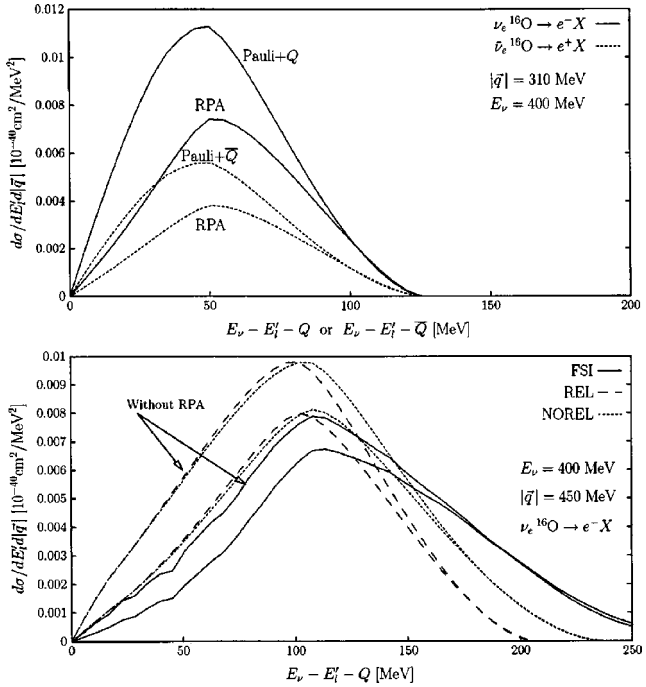

FIG. 13. ν_e and $\overline{\nu_e}$ differential cross sections in ^{16}O as a function of the excitation energy, for fixed values of the momentum transfer and $E_{\nu,\overline{\nu}}$=400 MeV. Top: Results obtained from the full relativistic model without FSI, with (RPA) and without RPA and Coulomb corrections **(**Pauli+$Q(\overline{Q})$**)**. Bottom: Results obtained by using relativistic (long dashed line, REL) and nonrelativistic nucleon kinematics. In this latter case, we present results with (solid line, FSI) and without (short dashed line, NOREL) FSI effects. For the three cases, we also show the effect of taking into account RPA and Coulomb corrections (lower lines at the peak). The areas (in units of 10^{-40} cm^2/MeV) below the curves are 1.02 (REL), 1.13 (NOREL), and 1.01 (FSI) when RPA and Coulomb corrections are not considered, and 0.79 (REL), 0.90 (NOREL), and 0.85 (FSI) when these nuclear effects are taken into account.

fied (a reduction of about 2.5% when RPA corrections are not considered and only about 1% enhancement when they are included).

In Fig. 13 we plot double differential cross sections for fixed momentum transfer, as a function of the excitation energy. We show neutrino and antineutrino cross sections from ^{16}O. FSI effects are not considered in the top panel, and one finds the usual QE shape, with peaks placed, up to relativistic corrections, in the neighborhood of $\vec{q}^2/2M$. Once more, medium polarization effects are clearly visible. FSI corrections are studied in the bottom panel, and we find the expected broadening of the QE peak, but the integrated cross sections remain almost unaltered.

Finally, in Table IV we compile muon and electron neutrino and antineutrino inclusive QE integrated cross sections from oxygen. We present results for relativistic and nonrelativistic nucleon kinematics and in this latter case, we present results with and without FSI effects. Though FSI changes importantly the shape of the differential cross sections, it plays a minor role when one considers total cross sections. When medium polarization effects are not considered, FSI provides significant reductions (13–29 %) of the cross sections [28]. However, when RPA corrections are included the reductions becomes more moderate, always smaller than 7%, and even there exist some cases where FSI enhances the cross sections. This can be easily understood by looking at Fig. 14, where we show the differential cross section as a function of the energy transfer for E_ν=375 MeV. There, we see that FSI increases the cross section for high energy transfer. But for nuclear excitation energies higher than those around the QE peak, the RPA corrections are certainly less important than in the peak region. Hence, the RPA suppression of the FSI distribution is significantly smaller than the RPA reduction of the distribution determined by the ordinary Lindhard function.

VII. CONCLUSIONS

The model presented in this paper, which is a natural extension of previous works [3–6] on electron, photon, and

TABLE IV. Muon (top) and electron (bottom) neutrino (left) and antineutrino (right) inclusive QE integrated cross sections from oxygen. We present results for relativistic (REL) and nonrelativistic nucleon kinematics. In this latter case, we present results with (FSI) and without (NOREL) FSI effects. Results, denoted as RPA and Pauli$Q(\overline{Q})$ have been obtained with and without including RPA correlations and Coulomb corrections, respectively.

		$\sigma(^{16}\mathrm{O}(\nu_\mu,\mu^- X))$ $(10^{-40}$ cm$^2)$			$\sigma(^{16}\mathrm{O}(\overline{\nu}_\mu,\mu^+ X))$ $(10^{-40}$ cm$^2)$		
E_ν (MeV)		REL	NOREL	FSI	REL	NOREL	FSI
500	Pauli+$Q(\overline{Q})$	460.0	497.0	431.6	155.8	168.4	149.9
	RPA	375.5	413.0	389.8	113.4	126.8	129.7
375	Pauli+$Q(\overline{Q})$	334.6	354.8	292.2	115.1	122.6	105.0
	RPA	243.1	263.9	243.9	79.8	87.9	87.5
250	Pauli+$Q(\overline{Q})$	155.7	162.2	122.5	63.4	66.4	52.8
	RPA	94.9	101.9	93.6	38.8	42.1	40.3
E_ν (MeV)		$\sigma(^{16}\mathrm{O}(\nu_e,e^- X))$ $(10^{-40}$ cm$^2)$			$\sigma(^{16}\mathrm{O}(\overline{\nu}_e,e^+ X))$ $(10^{-40}$ cm$^2)$		
		REL	NOREL	FSI	REL	NOREL	FSI
310	Pauli+$Q(\overline{Q})$	281.4	297.4	240.6	98.1	104.0	87.2
	RPA	192.2	209.0	195.2	65.9	72.4	73.0
220	Pauli+$Q(\overline{Q})$	149.5	156.2	121.2	60.7	63.6	51.0
	RPA	90.1	97.3	92.8	36.8	40.0	40.2
130	Pauli+$Q(\overline{Q})$	37.0	38.3	28.8	21.1	21.9	16.9
	RPA	20.6	22.3	23.3	10.9	11.9	12.8

pion dynamics in nuclei, should be able to describe inclusive QE neutrino and antineutrino nuclear reactions at intermediate energies of interest for future neutrino oscillation experiments. Even though the scarce existing data involve very low nuclear excitation energies, for which specific details of the nuclear structure might play a role, our model provides one of the best existing combined description of the inclusive muon capture in ^{12}C and of the measurements of the ^{12}C $(\nu_\mu,\mu^-)X$ and ^{12}C $(\nu_e,e^-)X$ reactions near threshold. Inclusive muon capture from other nuclei is also successfully described by the model.

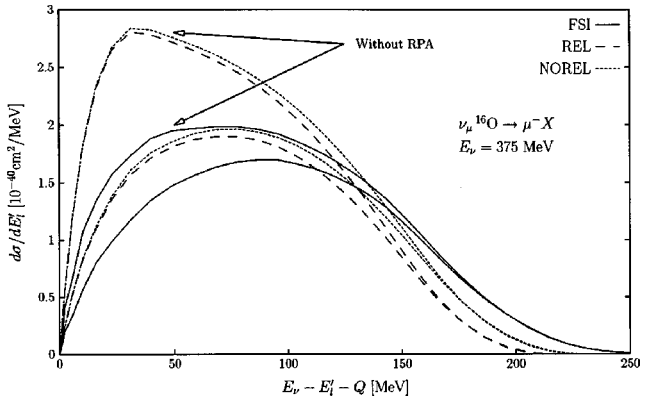

FIG. 14. Muon neutrino QE differential cross sections in oxygen as a function of the energy transfer. The neutrino energy is 375 MeV. We show results for relativistic (long dashed line, REL) and nonrelativistic nucleon kinematics. In this latter case, we present results with (solid line, FSI) and without (short dashed line, NOREL) FSI effects. We also show the effect of RPA and Coulomb corrections (lower lines at the peak). The integrated cross sections can be found in Table IV.

The inclusion of RPA effects, in particular the nuclear renormalization of the axial current, turned out to be extremely important to obtain an acceptable description of data. This had been already pointed out in Refs. [12,16,18,21], and it is a distinctive feature of nuclear reactions at intermediate energies [3–6]. On the other hand, FSI effects, though they produce significant changes in the shape of differential cross sections, lead to minor changes for integrated cross sections, comparable to the theoretical uncertainties, once RPA corrections are also taken into account.

The natural extension of this work is the study of higher transferred energies to the nucleus, also relevant for the analysis of future experiments that aim to determine the neutrino oscillation parameters with high precision. For those energies, the production of real pions and the excitation of the $\Delta(1232)$ or higher resonances will be contributions to the inclusive neutrino-nucleus cross section comparable to the QE one, or even larger.

ACKNOWLEDGMENTS

J.N. warmly thanks E. Oset for various stimulating discussions and communications. This work was supported by DGI and FEDER funds, contract BFM2002-03218, and by the Junta de Andalucía.

APPENDIX A: CC NUCLEON TENSOR

Impulse approximation

Performing the traces in Eq. (27) and taking into account that in Eq. (28) both the particle and the hole nucleons are on the mass shell $(p^2=(p+q)^2=M^2, 2p\cdot q+q^2=0)$, one finds

$$\begin{aligned}A^{\mu\nu}(p,q) &= 16(F_1^V)^2\left\{(p+q)^\mu p^\nu + (p+q)^\nu p^\mu + \frac{q^2}{2}g^{\mu\nu}\right\}\\ &+ 2q^2(\mu_V F_2^V)^2\left\{4g^{\mu\nu} - 4\frac{p^\mu p^\nu}{M^2} - 2\frac{p^\mu q^\nu + q^\mu p^\nu}{M^2}\right.\\ &\left. - q^\mu q^\nu\left(\frac{4}{q^2}+\frac{1}{M^2}\right)\right\} - 16F_1^V\mu_V F_2^V(q^\mu q^\nu - q^2 g^{\mu\nu})\\ &+ 4G_A^2\left\{2p^\mu p^\nu + q^\mu p^\nu + p^\mu q^\nu + g^{\mu\nu}\left(\frac{q^2}{2}-2M^2\right)\right.\\ &\left. - \frac{2M^2(2m_\pi^2-q^2)}{(m_\pi^2-q^2)^2}q^\mu q^\nu\right\} - 16iG_A(\mu_V F_2^V + F_1^V)\\ &\times\epsilon^{\mu\nu\alpha\beta}q_\alpha p_\beta. \end{aligned} \tag{A1}$$

The above tensor admits a decomposition of the type

$$\begin{aligned}A^{\mu\nu}(p,q) &= a_1 g^{\mu\nu} + a_2\left(p^\mu p^\nu + \frac{p^\mu q^\nu + p^\nu q^\mu}{2}\right) + ia_3\epsilon^{\mu\nu\alpha\beta}p_\alpha q_\beta\\ &+ a_4 q^\mu q^\nu \end{aligned} \tag{A2}$$

and from Eq. (A1) we have

$$a_1(q^2) = 8q^2\left\{(F_1^V+\mu_V F_2^V)^2 + G_A^2\left(\frac{1}{4}-\frac{M^2}{q^2}\right)\right\},$$

$$a_2(q^2) = 32(F_1^V)^2 - 8(\mu_V F_2^V)^2\frac{q^2}{M^2} + 8G_A^2,$$

$$a_3(q^2) = 16G_A(F_1^V+\mu_V F_2^V),$$

$$\begin{aligned}a_4(q^2) &= -\frac{8q^2}{M^2}(\mu_V F_2^V)^2\left(\frac{M^2}{q^2}+\frac{1}{4}\right) - \frac{8M^2G_A^2}{m_\pi^2-q^2}\left(\frac{q^2}{m_\pi^2-q^2}+2\right)\\ &- 16F_1^V\mu_V F_2^V. \end{aligned} \tag{A3}$$

RPA corrections

Taking $\vec{q}$ in the z direction and after performing the RPA sum of Fig. 3, we find, neglecting[22] corrections of order $O(k_F\vec{p}^2/M^2, k_F\vec{p}'^2/M^2, k_F q^0/M)$

$$\begin{aligned}\frac{A^{00}_{\rm RPA}}{4M^2} &= 8(F_1^V)^2\left\{\mathbf{C_N}\left(\frac{E(\vec{p})}{M}\right)^2 + \frac{q^2/4+q^0E(\vec{p})}{M^2}\right\}\\ &- 2\frac{q^2}{M^2}(\mu_V F_2^V)^2\left\{\frac{\vec{p}^2+q^0E(\vec{p})+(q^0)^2/4}{M^2} + \frac{(q^0)^2}{q^2}\right\}\\ &- 4\mathbf{C_N}F_1^V\mu_V F_2^V\frac{\vec{q}^2}{M^2} + 2G_A^2\left\{\frac{q^0E(\vec{p})+q^2/4+\vec{p}^2}{M^2}\right.\\ &\left. - \mathbf{C_L}\frac{(q^0)^2}{m_\pi^2-q^2}\left(\frac{q^2}{m_\pi^2-q^2}+2\right)\right\}, \end{aligned} \tag{A4}$$

$$\begin{aligned}\frac{A^{0z}_{\rm RPA}}{4M^2} &= 4(F_1^V)^2\left\{\mathbf{C_N}\frac{E(\vec{p})}{M}\frac{2p_z+|\vec{q}|}{M} + \frac{q^0p_z}{M^2}\right\}\\ &- \frac{q^2}{M^2}(\mu_V F_2^V)^2\left\{\frac{E(\vec{p})}{M}\frac{2p_z+|\vec{q}|}{M} + 2\frac{q^0|\vec{q}|}{q^2}\right.\\ &\left. + \frac{q^0(2p_z+|\vec{q}|)}{2M^2}\right\} - 4F_1^V\mu_V F_2^V\frac{q^0|\vec{q}|}{M^2}\\ &+ 2G_A^2\left\{\mathbf{C_L}\frac{E(\vec{p})}{M}\frac{2p_z+|\vec{q}|}{2M} + \frac{q^0p_z}{2M^2}\right.\\ &\left. - \mathbf{C_L}\frac{q^0|\vec{q}|}{m_\pi^2-q^2}\left(\frac{q^2}{m_\pi^2-q^2}+2\right)\right\}, \end{aligned} \tag{A5}$$

$$\begin{aligned}\frac{A^{zz}_{\rm RPA}}{4M^2} &= 8(F_1^V)^2\left\{\frac{p_z^2+|\vec{q}|p_z-q^2/4}{M^2}\right\}\\ &- 2\frac{q^2}{M^2}(\mu_V F_2^V)^2\left\{\left(\frac{2p_z+|\vec{q}|}{2M}\right)^2 + \frac{(q^0)^2}{q^2}\right\}\\ &- 4\left(\frac{q^0}{M}\right)^2F_1^V\mu_V F_2^V + 2G_A^2\left\{\mathbf{C_L} + \frac{p_z^2+|\vec{q}|p_z-q^2/4}{M^2}\right.\\ &\left. - \mathbf{C_L}\frac{\vec{q}^2}{m_\pi^2-q^2}\left(\frac{q^2}{m_\pi^2-q^2}+2\right)\right\}, \end{aligned} \tag{A6}$$

$$\begin{aligned}\frac{A^{xx}_{\rm RPA}}{4M^2} &= 8(F_1^V)^2\left\{\frac{p_x^2-q^2/4}{M^2}\right\} - 2\frac{q^2}{M^2}(\mu_V F_2^V)^2\left\{\mathbf{C_T} + \frac{p_x^2}{M^2}\right\}\\ &- 4\mathbf{C_T}\frac{q^2}{M^2}F_1^V\mu_V F_2^V + 2G_A^2\left\{\mathbf{C_T} + \frac{p_x^2-q^2/4}{M^2}\right\}, \end{aligned} \tag{A7}$$

$$\frac{A^{xy}_{\rm RPA}}{4M^2} = 4iG_A(F_1^V+\mu_V F_2^V)\left(\frac{q^0p_z}{M^2} - \mathbf{C_T}\frac{|\vec{q}|E(\vec{p})}{M^2}\right), \tag{A8}$$

with the polarization coefficients defined as

[22] Note that q^0/M is of the order $|\vec{q}|^2/M^2$ and as mentioned in Sec. III A, we have considered $\mu_V F_2^V|\vec{q}|/M$ of order $O(0)$

$$\mathbf{C_N}(\rho) = \frac{1}{|1 - c_0 f'(\rho) U_N(q,k_F)|^2},$$

$$\mathbf{C_T}(\rho) = \frac{1}{|1 - U(q,k_F) V_t(q)|^2}, \tag{A9}$$

$$\mathbf{C_L}(\rho) = \frac{1}{|1 - U(q,k_F) V_l(q)|^2}.$$

In order to preserve a Lorentz structure of the type $q^\mu q^\nu$, for the pseudoscalar-pseudoscalar and pseudoscalar–axial vector terms of the CC nucleon tensor, we have kept the RPA correction to the term

$$\frac{(q^0)^2}{m_\pi^2 - q^2}\left(\frac{q^2}{m_\pi^2 - q^2} + 2\right)$$

in A^{00}_{RPA}, despite behaving like $(q^0/|\vec{q}|)^2 \approx O(\vec{q}^2/M^2)$.

APPENDIX B: BASIC INTEGRALS

In a nonsymmetric nuclear medium, the relativistic Lindhard function is defined as

$$\overline{U}_R(q,k_F^n,k_F^p) = 2\int \frac{d^3p}{(2\pi)^3}\frac{M}{E(\vec{p})}\frac{M}{E(\vec{p}+\vec{q})}\frac{\Theta(k_F^n - |\vec{p}|)\Theta(|\vec{p}+\vec{q}| - k_F^p)}{q^0 + E(\vec{p}) - E(\vec{p}+\vec{q}) + i\epsilon} + (q \to -q). \tag{B1}$$

The two contributions above correspond to the direct and the crossed ph excitation terms, respectively. For positive transferred energy only the direct term has imaginary part, which is given by

$$\mathrm{Im}\,\overline{U}_R(q,k_F^n,k_F^p) = \int d^3p \mathcal{F}_R(q,\vec{p},k_F^n,k_F^p) = -M^2\frac{\Theta(q^0)\Theta(-q^2)}{2\pi|\vec{q}|}\Theta(E_F^n - E_F^p + q^0) \times \Theta(E_F^n - \mathcal{E}_R^p)(E_F^n - \mathcal{E}_R^p) \tag{B2}$$

with

$$\mathcal{F}_R(q,\vec{p},k_F^n,k_F^p) = -\frac{M^2}{4\pi^2}\frac{\Theta(q^0)\delta(q^0 + E(\vec{p}) - E(\vec{p}+\vec{q}))}{E(\vec{p})E(\vec{p}+\vec{q})} \times \Theta(k_F^n - |\vec{p}|)\Theta(|\vec{p}+\vec{q}| - k_F^p), \tag{B3}$$

$$\mathcal{E}_R^p = \mathrm{Max}\left\{M, E_F^p - q^0, \frac{-q^0 + |\vec{q}|\sqrt{1 - 4M^2/q^2}}{2}\right\}, \tag{B4}$$

$$E_F^{n,p} = \sqrt{M^2 + (k_F^{n,p})^2},$$

with Max$\{\cdots\}$ being the maximum of the quantities included in the bracket. To perform the d^3p integrations in Eqs. (28) and (62) is important to bear in mind that, though the LFG breaks down full Lorentz invariance, one still has rotational invariance; thus we find

$$T_R^0(q,k_F^n,k_F^p) = \int d^3p \mathcal{F}_R(q,\vec{p},k_F^n,k_F^p)E(\vec{p}) = \frac{1}{2}(E_F^n + \mathcal{E}_R^p)\mathrm{Im}\,\overline{U}_R(q,k_F^n,k_F^p), \tag{B5}$$

$$\vec{T}_R(q,k_F^n,k_F^p) = \int d^3p \mathcal{F}_R(q,\vec{p},k_F^n,k_F^p)\vec{p} = \left(\frac{q^2}{2|\vec{q}|^2}\,\mathrm{Im}\,\overline{U}_R(q,k_F^n,k_F^p) + \frac{q^0}{|\vec{q}|^2}T_R^0(q,k_F^n,k_F^p)\right)\vec{q}, \tag{B6}$$

$$R_R^{00}(q,k_F^n,k_F^p) = \int d^3p \mathcal{F}_R(q,\vec{p},k_F^n,k_F^p)E^2(\vec{p}) = \frac{1}{3}[(E_F^n)^2 + (\mathcal{E}_R^p)^2 + \mathcal{E}_R^p E_F^n]\mathrm{Im}\,\overline{U}_R(q,k_F^n,k_F^p), \tag{B7}$$

$$\vec{R}_R(q,k_F^n,k_F^p) = \int d^3p \mathcal{F}_R(q,\vec{p},k_F^n,k_F^p)E(\vec{p})\vec{p} = \left(\frac{q^2}{2|\vec{q}|^2}T_R^0(q,k_F^n,k_F^p) + \frac{q^0}{|\vec{q}|^2}R_R^{00}(q,k_F^n,k_F^p)\right)\vec{q}, \tag{B8}$$

$$R_R^{ij}(q,k_F^n,k_F^p) = \int d^3p \mathcal{F}_R(q,\vec{p},k_F^n,k_F^p)p^i p^j = \frac{a_R - b_R}{2}\delta^{ij} + \frac{3b_R - a_R}{2|\vec{q}|^2}q^i q^j,\ i,j = 1,2,3 \tag{B9}$$

with

$$a_R(q,k_F^n,k_F^p) = R_R^{00}(q,k_F^n,k_F^p) - M^2\,\mathrm{Im}\,\overline{U}_R(q,k_F^n,k_F^p), \tag{B10}$$

$$b_R(q,k_F^n,k_F^p) = \frac{1}{4|\vec{q}|^2}\{q^4\,\mathrm{Im}\,\overline{U}_R(q,k_F^n,k_F^p) + 4(q^0)^2 R_R^{00}(q,k_F^n,k_F^p) + 4q^2 q^0 T_R^0(q,k_F^n,k_F^p)\}. \tag{B11}$$

APPENDIX C: NONRELATIVISTIC REDUCTION OF THE RESULTS OF APPENDIX B

We take a nonrelativistic reduction of the nucleon dispersion relation

$$E(\vec{p}) \approx M + \frac{\vec{p}^2}{2M} \equiv \overline{E}(\vec{p}), \tag{C1}$$

which implies, for consistency, that in the definition of the imaginary part of the Lindhard function and in all integrals given in Appendix B the factors $M/E(\vec{p})$ and $M/E(\vec{p}+\vec{q})$

should be approximated by one. Thus, we have[23]

$$\overline{U}(q,k_F^n,k_F^p) = 2\int \frac{d^3p}{(2\pi)^3}\frac{\Theta(k_F^n-|\vec{p}|)\Theta(|\vec{p}+\vec{q}|-k_F^p)}{q^0+\overline{E}(\vec{p})-\overline{E}(\vec{p}+\vec{q})+i\epsilon} + (q\to -q) \tag{C2}$$

which correspond to the direct and the crossed ph excitation terms, respectively.[24] For positive values of q^0 we have

$$\text{Im}\,\overline{U}(q,k_F^n,k_F^p) = \int d^3p\mathcal{F}(q,\vec{p},k_F^n,k_F^p) = -M^2\frac{\Theta(q^0)\Theta(-q^2)}{2\pi|\vec{q}|}\Theta(\overline{E_F^n}-\overline{E_F^p}+q^0) \times\Theta(\overline{E_F^n}-\mathcal{E}^p)(\overline{E_F^n}-\mathcal{E}^p) \tag{C3}$$

with

$$\mathcal{F}(q,\vec{p},k_F^n,k_F^p) = -\frac{1}{4\pi^2}\Theta(q^0)\delta(q^0+\overline{E}(\vec{p})-\overline{E}(\vec{p}+\vec{q})) \times\Theta(k_F^n-|\vec{p}|)\Theta(|\vec{p}+\vec{q}|-k_F^p), \tag{C4}$$

$$\mathcal{E}^p = \text{Max}\left\{\overline{E_F^p}-q^0, M+\frac{1}{2M}\left(\frac{Mq^0}{|\vec{q}|}-\frac{|\vec{q}|}{2}\right)^2\right\},$$

$$\overline{E_F^{n,p}} = M+\frac{(k_F^{n,p})^2}{2M}. \tag{C5}$$

To perform the integrations implicit in Eqs. (28) and (62) we need

$$T^0(q,k_F^n,k_F^p) = \int d^3p\mathcal{F}(q,\vec{p},k_F^n,k_F^p)\overline{E}(\vec{p}) = \frac{1}{2}(\overline{E_F^n}+\mathcal{E}^p)\text{Im}\,\overline{U}(q,k_F^n,k_F^p) \tag{C6}$$

$$\vec{T}(q,k_F^n,k_F^p) = \int d^3p\mathcal{F}(q,\vec{p},k_F^n,k_F^p)\vec{p} = \left(-\frac{1}{2}+\frac{Mq^0}{|\vec{q}|^2}\right)\text{Im}\,\overline{U}(q,k_F^n,k_F^p)\vec{q}, \tag{C7}$$

$$R^{00}(q,k_F^n,k_F^p) = \int d^3p\mathcal{F}(q,\vec{p},k_F^n,k_F^p)\overline{E^2}(\vec{p}) = \frac{1}{3}((\overline{E_F^n})^2+(\mathcal{E}^p)^2+\mathcal{E}^p\overline{E_F^n})\text{Im}\,\overline{U}(q,k_F^n,k_F^p), \tag{C8}$$

$$\vec{R}(q,k_F^n,k_F^p) = \int d^3p\mathcal{F}(q,\vec{p},k_F^n,k_F^p)\overline{E}(\vec{p})\vec{p} = \left(\frac{Mq^0}{|\vec{q}|^2}-\frac{1}{2}\right)T^0(q,k_F^n,k_F^p)\vec{q}, \tag{C9}$$

$$R^{ij}(q,k_F^n,k_F^p) = \int d^3p\mathcal{F}(q,\vec{p},k_F^n,k_F^p)p^ip^j = \frac{a-b}{2}\delta^{ij}+\frac{3b-a}{2|\vec{q}|^2}q^iq^j,\ i,j=1,2,3 \tag{C10}$$

with

$$a(q,k_F^n,k_F^p) = 2M\{T^0(q,k_F^n,k_F^p)-M\,\text{Im}\,\overline{U}(q,k_F^n,k_F^p)\}, \tag{C11}$$

$$b(q,k_F^n,k_F^p) = \frac{1}{4|\vec{q}|^2}(2Mq^0-|\vec{q}|^2)^2\text{Im}\,\overline{U}(q,k_F^n,k_F^p). \tag{C12}$$

APPENDIX D: FREE NUCLEON CROSS SECTION

The cross section for the process $\nu_l+n\to l^-+p$ is given by

$$\sigma_{\nu l} = \frac{G^2\cos^2\theta_c}{8\pi(s-M^2)^2}\int_{q^2_{\min}}^{q^2_{\max}} dq^2 L_{\mu\nu}A^{\nu\mu}|_{p=(M,\vec{0})}, \tag{D1}$$

where the leptonic (L) and nucleon (A) tensors are defined in Eqs. (4) and Eqs. (27) and (A1), respectively, $q^2_{\min(\max)}=m_l^2-2E_\nu(E_l'\pm|\vec{k}'|)$ with E_ν and E_l', $\vec{k}'$ the incoming neutrino laboratory energy and outgoing lepton laboratory energy and momentum, and finally $s=(2E_\nu+M)M$. The variable q^2 is related to the outgoing lepton laboratory polar angle (θ') by $q^2=(k-k')^2=m_l^2-2E_\nu(E_l'-|\vec{k}'|\cos\theta')$. The tensor contraction in Eq. (D1) gives in the laboratory frame:

$$L_{\mu\nu}A^{\nu\mu}|_{p=(M,\vec{0})} = (q^2-m_l^2)\left\{a_1+\frac{s}{2}a_2-\frac{q^2}{2}a_3-a_4\frac{m_l^2}{2}\right\} + (s-M^2)\left\{\frac{s-M^2}{2}a_2-q^2a_3\right\} \tag{D2}$$

with the nucleon structure functions, $a_i(q^2)$, given in Eq. (A3). The cross section for the process $\overline{\nu_l}+p\to l^++n$ is obtained from Eqs. (D1) and (D2) by replacing a_3 by $-a_3$.

[23] We suppress the subindex R to distinguish the new expressions from the former ones.

[24] For symmetric nuclear matter $\rho_p=\rho_n=\rho$, the above expression coincides, up to a factor 2 due to isospin, with the definition of U_N given in Eq. (2.9) of Ref [35].

[1] See for instance, talks at The Third Workshop on Neutrino-Nucleus Interactions in the Few GeV Region (NuInt04), http://nuint04.lngs.infn.it, Gran Sasso, 2004.

[2] Y. Fukuda *et al.*, Phys. Rev. Lett. **81**, 1562 (1998).

[3] R.C. Carrasco and E. Oset, Nucl. Phys. **A536**, 445 (1992); R.C. Carrasco, E. Oset, and L.L. Salcedo, *ibid.* **A541**, 585 (1992); R.C. Carrasco, M.J. Vicente-Vacas, and E. Oset, *ibid.* **A570**, 701 (1994).

[4] A. Gil, J. Nieves, and E. Oset, Nucl. Phys. **A627**, 543 (1997); **A627**, 599 (1997).

[5] E. Oset, H. Toki, and W. Weise, Phys. Rep. **83**, 281 (1982).

[6] L.L. Salcedo, E. Oset, M.J. Vicente-Vacas, and C. García Recio, Nucl. Phys. **A484**, 557 (1988); C. García-Recio *et al.*, *ibid.* **A526**, 685 (1991); J. Nieves, E. Oset, and C. García-Recio, *ibid.* **A554**, 509 (1993); **A554**, 554 (1993); E. Oset *et al.*, Prog. Theor. Phys. Suppl. **117**, 461 (1994); C. Albertus, J.E. Amaro, and J. Nieves, Phys. Rev. Lett. **89**, 032501 (2002); Phys. Rev. C **67**, 034604 (2003).

[7] J. Nieves, J.E. Amaro, and M. Valverde, nucl-th/0408008, talk given at The Third Workshop on Neutrino-Nucleus Interactions in the Few GeV Region, Gran Sasso, 2004.

[8] H. Primakoff, Rev. Mod. Phys. **31**, 802 (1959).

[9] N.C. Mukhopadhyay, Phys. Rep., Phys. Lett. **30**, 1 (1977).

[10] N. Van Giai, N. Auerbach, and A.Z. Mekjian, Phys. Rev. Lett. **46**, 1444 (1981).

[11] J. Navarro, J. Bernabéu, J.M.G. Gómez, and J. Martorell, Nucl. Phys. **A375**, 361 (1982).

[12] H.C. Chiang, E. Oset, and P. Fernández de Córdoba, Nucl. Phys. **A510**, 591 (1990); N.C. Mukhopadhyay, H.C. Chiang, S.K. Singh, and E. Oset, Phys. Lett. B **434**, 7 (1998).

[13] E. Kolbe, K. Langanke, and P. Vogel, Phys. Rev. C **50**, 2576 (1994); **62**, 055502 (2000).

[14] C.W. Kim and S.L. Mintz, Phys. Rev. C **31**, 274 (1985).

[15] A.C. Hayes and I.S. Towner, Phys. Rev. C **61**, 044603 (2000).

[16] N. Auerbach and B.A. Brown, Phys. Rev. C **65**, 024322 (2002).

[17] N. Jachowicz, K. Heyde, J. Ryckebusch, and S. Rombouts, Phys. Rev. C **65**, 025501 (2002).

[18] E. Kolbe, K. Langanke, G. Martínez-Pinedo, and P. Vogel, J. Phys. G **29**, 2569 (2003).

[19] T.K. Gaisser and J.S. O'Connell, Phys. Rev. D **34**, 822 (1986).

[20] T. Kuramoto, M. Fukugita, Y. Kohyama, and K. Kubodera, Nucl. Phys. **A512**, 711 (1990).

[21] S.K. Singh and E. Oset, Nucl. Phys. **A542**, 587 (1992); Phys. Rev. C **48**, 1246 (1993); T.S. Kosmas and E. Oset, *ibid.* **53**, 1409 (1996); S.K. Singh, N.C. Mukhopadhyay, and E. Oset, *ibid.* **57**, 2687 (1998).

[22] S.L. Mintz and M. Pourkaviani, Nucl. Phys. **A594**, 346 (1995).

[23] Y. Umino and J.M. Udias, Phys. Rev. C **52**, 3399 (1995); Y. Umino, J.M. Udias, and P.J. Mulders, Phys. Rev. Lett. **74**, 4993 (1995).

[24] E. Kolbe, K. Langanke, F.K. Thielemann, and P. Vogel, Phys. Rev. C **52**, 3437 (1995); E. Kolbe, K. Langanke, and S. Krewald, *ibid.* **49**, 1122 (1994); E. Kolbe, K. Langanke, and P. Vogel, Nucl. Phys. **A613**, 382 (1997); **A652**, 91 (1999).

[25] N. Auerbach, N. Van Giai, and O.K. Vorov, Phys. Rev. C **56**, R2368 (1997); N. Auerbach *et al.*, Nucl. Phys. **A687**, 289c (2001).

[26] W.M. Alberico *et al.*, Nucl. Phys. **A623**, 471 (1997); Phys. Lett. B **438**, 9 (1998); Nucl. Phys. **A651**, 277 (1999).

[27] C. Volpe *et al.*, Phys. Rev. C **62**, 015501 (2000).

[28] C. Bleve *et al.*, Astropart. Phys. **16**, 145 (2001).

[29] C. Maieron, M.C. Martinez, J.A. Caballero, and J.M. Udias, Phys. Rev. C **68**, 048501 (2003).

[30] A. Meucci, C. Giusti, and F.D. Pacati, Nucl. Phys. **A739**, 277 (2004).

[31] K. M. Graczyk, nucl-th/0401053.

[32] S. Galster *et al.*, Nucl. Phys. **B32**, 221 (1971).

[33] J. Speth, E. Werner, and W. Wild, Phys. Rep. **33**, 127 (1977); J. Speth, V. Klemt, J. Wambach, and G.E. Brown, Nucl. Phys. **A343**, 382 (1980).

[34] D.H. Wilkinson, Nucl. Phys. **A209**, 470 (1973); **A225**, 365 (1974).

[35] C. García-Recio, E. Oset, and L.L. Salcedo, Phys. Rev. C **37**, 194 (1988).

[36] J. Engel, Phys. Rev. C **57**, 2004 (1998).

[37] H. Behrens and W Bühring, *Electron Radial Wave Functions and Nuclear Beta Decay* (Clarendon, Oxford, 1982).

[38] C. Itzykson and J. B. Zuber, *Quantum Field Theory* (McGraw-Hill, New York, 1980).

[39] P. Fernández de Córdoba and E. Oset, Phys. Rev. C **46**, 1697 (1992).

[40] A. Ramos, A. Polls, and W. H. Dickhoff, Nucl. Phys. **A503**, 1 (1989).

[41] H. Müther, G. Knehr, and A. Polls, Phys. Rev. C **52**, 2955 (1995).

[42] L.L. Salcedo *et al.*, Phys. Lett. B **208**, 339 (1988).

[43] C. Ciofi degli Atti, S. Liuti, and S. Simula, Phys. Rev. C **41**, 2474 (1990).

[44] R.B. Firestone, *Table of Isotopes*, 8th ed. (Wiley, New York, 1996).

[45] C.W. de Jager, H. de Vries, and C. de Vries, At. Data Nucl. Data Tables **14**, 479 (1974); **36**, 495 (1987).

[46] J.W. Negele and D. Vautherin, Phys. Rev. C **11**, 1031 (1975), and references therein.

[47] C. García-Recio, J. Nieves, and E. Oset, Nucl. Phys. **A547**, 473 (1992).

[48] J.E. Amaro, C. Maieron, J. Nieves, and M. Valverde, nucl-th/0409017.

[49] J.E. Amaro, A.M. Lallena, and J. Nieves, Nucl. Phys. **A623**, 529 (1997); H.C. Chiang *et al.*, *ibid.* **A510**, 573 (1990); **A514**, 749(E) (1990).

[50] M. Albert *et al.*, Phys. Rev. C **51**, R1065 (1995).

[51] C. Athanassopoulos *et al.*, Phys. Rev. C **56**, 2806 (1997).

[52] L.B. Auerbach *et al.*, Phys. Rev. C **66**, 015501 (2002).

[53] B. Zeitnitz, Prog. Part. Nucl. Phys. **32**, 351 (1994); B.E. Bodmann *et al.*, Phys. Lett. B **332**, 251 (1994).

[54] C. Athanassopoulos *et al.*, Phys. Rev. C **55**, 2078 (1997).

[55] D.A. Krakauer *et al.*, Phys. Rev. C **45**, 2450 (1992).

[56] T. Suzuki, D.F. Measday, and J.P. Roalsvig, Phys. Rev. C **35**, 2212 (1987) and references therein.